

**ANALYSIS AND DESIGN OF INDUCTIVE POWER
TRANSFER SYSTEMS FOR AUTOMOTIVE BATTERY
CHARGING APPLICATIONS**

**A THESIS SUBMITTED TO THE GRADUATE
SCHOOL OF APPLIED SCIENCES
OF
NEAR EAST UNIVERSITY**

**By
WAHAB ALI SHAH**

**In Partial Fulfillment of the Requirements for
the Degree of Master of Science
in
Electrical and Electronic Engineering**

NICOSIA, 2016

I hereby declare that all information in this document has been obtained and presented in accordance with academic rules and ethical conduct. I also declare that, as required by these rules and conduct, I have fully cited and referenced all material and results that are not original to this work.

Name: Wahab Ali Shah

Signature:

Date:

ACKNOWLEDGEMENTS

More than something else, I offer my humble thanks to ALLAH Almighty for bestowing upon me and giving me the potential for the completion of this research work. My special praise to Prophet Muhammad (Peace be upon him) who is forever a source of guidance for the humanity as a whole.

I would like to express my deep and sincere gratitude to my supervisor, Associate Prof. Dr. Timur Aydemir for his supervision, advice, understanding and keeping encourage from the very early stage of the dissertation.

I would also like to express my sincere thanks to Mr. Faisal who is a PhD candidate and part time lecturer at Near East University, North Cyprus. His wisdom, knowledge and commitment to the highest standards have inspired and motivated me and guided me to the right path. I am thankful to the other staff members in my department.

I wish to thank my family members and friends especially my parents who always supported and encouraged me in all aspects of my life.

In the end I would like to pay my regards gratitude and thanks to my loving wife, without her inspiration and motivation it would be impossible for me to complete this study.

To my parents....

ABSTRACT

Transferring electrical power without any wiring has been a dream since late 19th century when Tesla first came up with the idea. There were some advances in this area in 1950s after scientists learned more about microwave systems. However, this subject has recently become very attractive after scientists in MIT announced their practical systems. Today, there are several research projects all around world at the universities and industry to utilize this concept. There are low power applications such as charging the batteries of contactless tooth brushes or implanted devices, and higher power applications such as charging the batteries of electrical automobiles or buses. In the first group of applications operating frequencies are in microwave range while the frequency is lower in high power applications. In the latter the concept is also called inductive power transfer.

In this thesis an inductive power transfer system is studied. Operation principles of these systems are explained and components of the system are described. Coil design is one of the most critical tasks and a chapter is devoted for coil design. Also simulation results obtained for a 2 kW single phase system are given.

Keywords: Inductive power transfer; contactless charging; coil design; electrical automobiles; operating frequency

ÖZET

Elektrik enerjisinin herhangi bir kablo kullanmaksızın Tesla tarafından düşüncenin ilk ortaya atıldığı 19. Yüzyılın sonlarından beri herkesin rüyasıdır. 1950li yıllarda bilim insanlarının mikrodalga sistemleri hakkında bilgi sahibi olmasıyla bu alanda bazı ilerlemeler sağlandı. Ancak, konu son yıllarda MIT'deki araştırmacıların gerçekleştirdikleri sistemi duyurmasıyla birlikte çok ilgi çekmeye başlamıştır. Günümüzde dünyanın her yanında üniversitelerde ve sanayi kuruluşlarında bu kavramı kullanmak için projeler yapılmaktadır. Temassız dış fırçaları veya vücuda gömülü cihazların bataryalarını şarj etmek için kullanılan küçük güçlü sistemler gibi elektrikli otomobiller veya otobüslerin bataryalarını şarj etmek için kullanılan yüksek güçlü sistemler de bulunmaktadır. İlk grup uygulamalarda çalışma frekansı mikrodalga bölgesindeyken yüksek güçlü uygulamalarda frekans düşüktür. Bu ikinci sınıftaki kavrama Endüktif Güç Aktarımı adı da verilmektedir.

Bu tezde enfüktif güç sistemleri incelenmektedir. Bu sistemlerin çalışma ilkeleri incelenmekte bileşenleri tanıtılmaktadır. Sargı tasarımı endüktif güç aktarımı sistem tasarımının en kritik işlerinden biridir. Bu nedenle bu konuya bir bölüm ayrılmıştır. Ayrıca 2 kW gücünde tek fazlı örnek bir sistemin benzetim sonuçları verilmektedir.

Anahtar Kelimeler: Endüktif güç aktarımı; kablosuz şarj sistemleri; sargı tasarımı; elektrik otomobil; çalışma frekansı

TABLE OF CONTENTS

ACKNOWLEDGMENTS	iii
ABSTRACT	v
ÖZET	vi
TABLE OF CONTENTS	vii
LIST OF TABLES	ix
LIST OF FIGURES	x
LIST OF SYMBOLS	xii
LIST OF ABBREVIATIONS	xiii
 CHAPTER 1: INTRODUCTION	
1.1 The Aim of Thesis.....	2
1.2 Thesis Structure	2
 CHAPTER 2: GENERAL STRUCTURE INDUCTIVE POWER SYSTEM	
2.1 History of Inductive Power System.....	3
2.2 Inductive Power System.....	5
2.3 Types of Coils and Charging Distances	6
2.4 Compensation Topologies	10
2.5 Power Converters and its Control.....	16
 CHAPTER 3: PRINCIPLES OF INDUCTIVE POWER TRANSFER	
3.1 Inductive Power Transfer	18
3.2 Principle of Operation	19
3.3 Need of High Frequency.....	22
3.3.1 Material selection for coil	23
3.3.2 Material selection for core	23
3.4 Field Shaping Techniques.....	25
3.5 Compensation Systems.....	25

CHAPTER 4: DESIGN OF A COIL

4.1 Design Methodology.....	32
4.2 Results of MATLAB Code	39
4.3 Design 2kW System	42

CHAPTER 5: SIMULATION OF THE SYSTEM

5.1 Introduction.....	44
5.2 Single Phase Full Wave Inverter.....	44
5.3 Simulated Circuit.....	45
5.4 Simulated Results.....	46

CHAPTER 6: CONCLUSION AND FUTUREWORK

REFERENCES.....	51
------------------------	-----------

APPENDICES

Appendix 1: Calculations for Self & Mutual Inductance for Rectangular.....	54
Appendix 2: Overall MATLAB Code for Main Program.....	58
Appendix 3: MATLAB Code for Tables.....	60
Appendix 4: MATLAB Code for L and M Equations.....	61

LIST OF TABLES

Table 2.1: Some ICPT system examples with ferrite and air core.....	6
Table 2.2: Properties of compensation topologies.....	15
Table 3.1: Secondary coil ratings for maximum power transfer with resistive load.....	27
Table 4.1: Compensation capacitance values for all classical topologies.....	32
Table 4.2: Equations to calculate the electrical quantities each topology.....	33
Table 4.3: The ratio of the currents and efficiencies for each compensation topology...	34
Table 4.4: Results of coil parameters by using MATLAB Code.....	41
Table 5.1: Combinations of switches and output voltage.....	43

LIST OF FIGURES

Figure 2.1:	Charging type.....	5
Figure 2.2:	IPT circuit	6
Figure 2.3:	Ferrite base.....	7
Figure 2.4:	Flux Pipe charge pad flux distribution	8
Figure 2.5:	DD charge pad flux distribution.....	9
Figure 2.6:	DDQ charge pad	10
Figure 2.7:	Series-series compensation model.....	11
Figure 2.8:	Series parallel topology compensation model.....	12
Figure 2.9:	Parallel series compensation model.....	13
Figure 2.10:	Parallel-parallel topology compensation model.....	14
Figure 2.11:	Circuit diagram of a typical structure.....	16
Figure 3.1:	Series-series compensated ICPT.....	18
Figure 3.2:	Two uncompensated mutually-coupled air cored coils.....	19
Figure 3.3:	Electrical equivalent circuit of uncompensated mutually coupled coils.	20
Figure 3.4:	Current density distributions in copper wire.....	24
Figure 3.5:	Basic compensation topologies.....	26
Figure 3.6:	Series compensated secondary.....	27
Figure 4.1:	The flow chart for IPT system design proposed.....	31
Figure 4.2:	Copper-mass vs. $\ln Q_p/Q_s$	37
Figure 4.3:	Turn number variation for the primary at each step.....	39
Figure 4.4:	Turn number variation for the secondary at each step.....	40
Figure 4.5:	Cross-section area variation for the primary for each step (in mm^2).....	40

Figure 4.6: Cross-section area variation for the secondary for each step (in mm ²)..	41
Figure 4.7: Output power variation for each step (in kW).....	41
Figure 4.8: Variation of resonance frequency in kHz.....	42
Figure 5.1: Full wave bridge inverter.....	44
Figure 5.2: Simulated circuit.....	46
Figure 5.3: Inverter output voltages.....	47
Figure 5.4: Primary and secondary current.....	47
Figure 5.5: Capacitor voltages.....	48
Figure 5.6: Load voltage.....	49

LIST OF SYMBOLS

C_1 :	Capacitance value of primary side
C_2 :	Capacitance value of secondary side
h :	Distance between windings
I_1 :	Source current
I_2 :	Load current
I_{C1} :	Primary capacitor current
I_{C2} :	Secondary capacitor current
I_P :	Primary winding current
I_S :	Secondary winding current
L_1 :	Inductance value of primary winding
L_2 :	Inductance value of secondary winding
PP :	Parallel-parallel topology
PS :	Parallel-series topology
Q_P :	Quality factor value of the primary circuit
Q_S :	Quality factor value of the Secondary circuit
R_L :	Load resistance
S_1 :	Primary winding section
S_2 :	Secondary winding section
SP :	Series-parallel topology
SS :	Series-series topology
V_1 :	Input voltage
V_{C1} :	Primary capacitor

LIST OF ABBREVIATIONS

AC :	Alternating current
DC :	Direct current
EMI :	Electromagnetic induction
IEC :	International Electro technical Commission
IEEE :	Institute of Electrical and Electronics Engineers
IGBT :	Insulated gate bipolar transistor
k :	coupling coefficient
L :	Self inductance
M :	Mutual inductance
MOSFET :	metal–oxide–semiconductor field-effect transistor
N1 :	Number of turns in primary winding
N2 :	Number of turns in Secondary winding
P :	Active power
PF :	Power factor
PL :	Power transferred to secondary load
PWM :	Pulse width modulation
Q :	Reactive power
RMS :	Root mean square
S :	Apparent power
THD :	Total Harmonic distortion
UPS :	Uninterruptable Power Supply

CHAPTER 1

INTRODUCTION

The growing number of energy consuming devices, together with the increasing demand for energy, has led to an energy crisis in the world today. Furthermore, some petroleum products including liquefied petroleum gas and natural compressed gas have for several decades remained the main sources of energy for transportation. Because of the continuous carbon dioxide emission from the use of these energy sources, there is a steady increase in the global warming. This has compelled engineers and scientists, together with researchers to find an accurate and sustainable alternate solution to these natural energy sources.

To this effect, a lot of energy technologies are being developed and applied to avoid global warming from gas exhaustion and to reduce energy cost. The advent and EVs integration has been received by all as a present solution to the depleting assets (petroleum), which are mainly used in the automotive applications. The trend in the development of these advanced energy systems can be analyzed carefully. The concept of electric vehicles (EVs) was developed, through initiation of the “HEV” stands for hybrid electric vehicles. Shortly afterwards, Engineers took another step forward, with the invention of PHEVs (for plug-in) or connect HEV’s. Nonetheless, Plug-in hybrid electric vehicles were accepted, used the applications were associated with a lot of disadvantages. It was enhanced with the linking cable and charger (plug-in) as well as galvanic isolation of onboard electronics. Also it was difficult to carry the charger, given its size and weight. This system was associated with heavier problems, like operating it in rain and snow, since water is also a conductor that could cause the short circuiting of the system. To avoid these numerous setbacks in the PHEV, many technologies have been advanced, to produce pure EV. Pure EV has decent qualities. Unlike the conventional transport system, an electric vehicle (EV) enhances smoke free transport; as a result that describes a successful clarification to the unpleasant atmosphere impact (toxic smoke). Pure electric vehicles (EVs) have additional advantages. They can be powered through having large gap/ distance, by charging wirelessly, and does not depend upon weather conditions (good or bad) along with no connecting wires or plugs, such as in plug-in hybrid electric vehicles. EV also has limitations. Batteries used to store energy are heavy and

expensive. Time is needed to fully charge the batteries and the driving range is still limited. Also, batteries need to be replaced in a few years.

A recent topic of interest for EVs is wireless charging. It is also called inductive charging technology (IPT). Through IPT it is possible to charge batteries in shorter time without any physical correction. IPT can be used for static and dynamic charging. Although, it is a safe technology, there are issues to address such as alignment of coils, foreign object detection, and live object detection.

1.1. The Aim of the Thesis

The aim of the thesis is to have an overview of the inductive power transfer for electrical vehicles with a special concentration on coil design and power converter simulation for static charging.

Coil design is very important for an efficient and safe power transfer. Equations and techniques related to coil design are presented and discussed in the system. Power converters are used in both side of the system. The converter on the primary side is used to generate a high frequency voltage to excite the primary coil. The purpose of the converter in the secondary is to rectify the voltage transferred from the primary to charge the battery.

1.2. Thesis Structure

The rest of the thesis is organized as follows:

Chapter 2 provides a detailed explanation of the subject, and literature review.

Chapter 3 provides an overview of inductive power transfer systems.

Chapter 4 coil design procedure will be presented here.

Chapter 5 single phase full bridge dc-dc converter, simulation results obtained by MATLAB

Chapter 6 gives the conclusions

CHAPTER 2

GENERAL STRUCTURE OF INDUCTIVE POWER SYSTEM

2.1. History of Wireless Power Transfer

The advancement of knowledge through history does not take after one track. Rather, it is an endless group of minor commitments that drive humanity onward. Conversely, all historic period has had its own unique achievement that is somewhat more notable than others. For instance, the fifties were famous by the development of space study, whereas the end of the 20th century was well-known by the advancement of PCs and the start of the information age. Clearly, one of the symbols of the start of the 21st century is the quick evolution of wireless communication and flexibility. One cannot see life nowadays without mobile phones, portable PCs, worldwide positioning systems, etc.

In contrast to wireless information exchange, wireless power is an old idea Nikola Tesla tested in the late 1800's. He was considering it as a distinct option for building the electric grid. He designed the first systems and built a tower to test his system. However, funding was not enough and the project was suspended. The concept became a subject of interest again after the Second World War with the advent of microwave systems.

William et al. (1963) demonstrated the first microwave wireless power transmission system. Brown subsequently generated his idea and wirelessly powered a model helicopter.

History states that wireless power were never acknowledged at a customer level and the idea was nearly overlooked. In 2007 researchers at MIT issued an official statement representing how to transfer power wirelessly using magnetic resonance and introduced results of transfer distances up to two or three meters. Then interest in this technology has boomed and it is easy to see why. Wireless power might be used in a wide-ranging of applications stretching from mobile devices cell phones, tablets, laptops, and sensors to plug-in cars, transports. Estimations demonstrate that wireless power could be a billion-dollar industry within the coming 10 years. In short, inductive power transfer also called wireless power transfer. It is

the transmission of electrical energy from the electrical source to electrical load without any connection. This technology is very valuable in those situations where uses of interconnecting wires are difficult, hazardous/dangerous, or almost unmanageable. IPT can be utilized as a part of numerous applications like hybrid electrical vehicle, medical sensor, laptop charger etc.

The first research project that looked at inductive charging with some details is the U.C Berkley PATH program in the late 1970s. The system has a limitation of a frequency of few hundred hertz. The system function as a spring board to a preliminary charging system of frequencies that is very high. Consequently, the system detuned and operated when placed next to the ferromagnetic chassis of the vehicle. Thereafter and more recently, a multipath receiver pickup was presented for inductive charging. Many other publications have been made on pad design (for vehicle charging). However, they have not provided a thorough overall design process. The limitation here is that the system efficiency is 85% with power level around 60 kW, researchers have started to experiment at in motion charging for light duty vehicles, though the research is still at its early stage as the full hardware solutions for the system is yet to be implemented (Hunter et al., 2012).

National University of Kyoto, Japan has repeatedly conducted research on Micro Power Transfer (MPT). In the year of **two-thousand**, researchers in **Kyoto University** established a system for MPT charging of EV's and they obtained 76% efficiency. Volvo technologies japan and Nilion Dengyo Kosaku companies developed 10kW retina array, which has receiving capability 3.2kW/m² at distance of 4meters, and obtained 84% efficiency. The MPT systems were shown by the above technologies to have the capabilities of transmitting power to long distance, but with the increased-cost disadvantage, and large antenna size. Likewise, high power applications (transmission through microwaves) have no security for human beings. However, available solutions exist to overcome this shortcoming of cost, along with antenna size (Kafeel et al., 2015).

The study related to the design techniques for magnetic coupler, mechanisms for control, detection-algorithms, compensation topologies, as well as safety issues (radiation). Amongst the several issues addressed above, researchers concluded on the design of magnetic coupler and compensation circuits. Loosely coupled transformer formed the magnetic couplers of

WPT chargers. They have their primary and secondary coils linked across a relatively large air gap in a fixed charging system. Having a higher efficiency and tolerance to misalignment with maximum dimensions, and cost is always preferable. In a bit to reach this goal, some other kinds of couplers, their geometries along with configurations have been proposed by researchers. Circular design has been well researched and optimized (Siqi et al., 2015).

2.2. Inductive Power Transfer (IPT)

Though the plug in electric vehicles was successful, it was always associated with a safety risk, due to the metal-to- metal direct contact. This safety risk was completely eliminated, through the design of charging EV’s structures based and organized by IPT.

In IPT system power is transferred from one coil to another coil through electromagnetic induction, through air-cored transformer and both coils closed-spaced coils are connected to one another apparently, but are isolated electrically. This can be demonstrated in the Figure 2.1(a) and (b) using a charging pad-type charger plug-in vehicle (fueling) likes convectional automobiles. IPT system block diagram is given in Figure 2.2. The method shows a high power-transfer with small air-gap among both coils. Furthermore, if air gap is larger/higher due to leakage inductance the efficiency η will be decreases and vice versa (Kafeel et al., 2015).



(a) Charging IPT

(b) Charging-pad

Figure 2.1: Charging type (Kafeel et al., 2015)

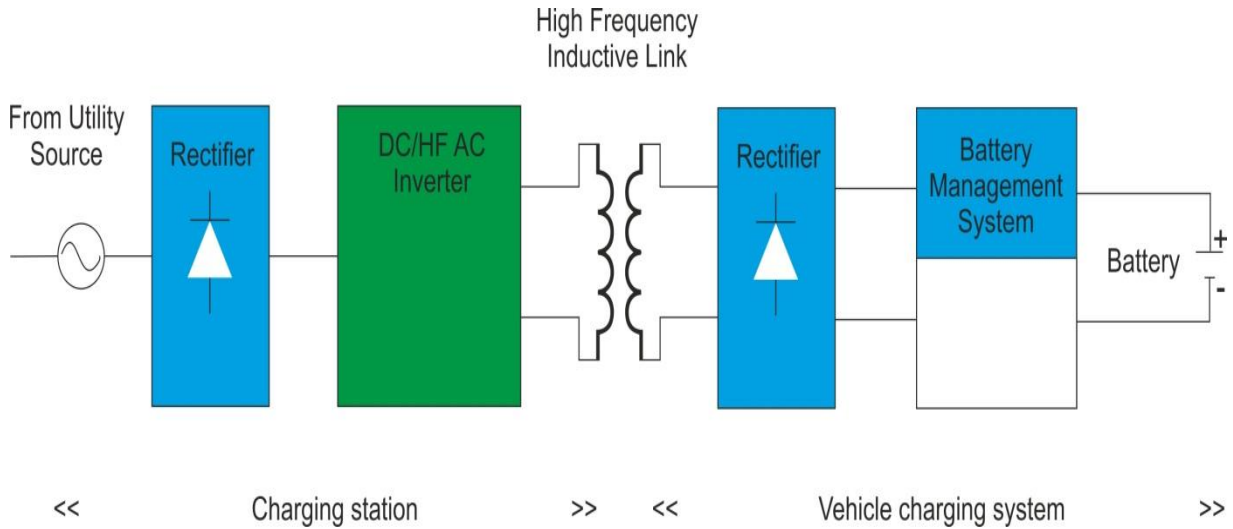


Figure 2.2: IPT circuit

2.3 Types of Coils and Charging Distances

The question arises how to get maximum efficiency (η) while transmitting high power to a load. Different designs suggest using ferrite cores or air core. The ferrite core is preferred because of having high coupling co-efficient and lower cost. Table 1 shows the specifications of some ICPT system examples with ferrite and air core.

Table 2.1: Some ICPT system examples with ferrite and air core

Ferrite Core systems		Air core systems	
Charging distance (mm)	Coupling co-efficient	Charging distance (mm)	Coupling co-efficient
70	0.35	200	0.16
80	0.25	2000	0.01
6	0.72	300	0.05

Different shapes are considered to get the maximum efficiency (η), and power. In the very early stages the shapes were like U-core, E-core and pot core. These types of shapes were not used properly because of greater thickness (Kafeel et al., 2015)

- **Single-sided Circular Charge Pad**

A single-sided circular charge pad topology has a ferrite base and magnetic flux which decreases the unwanted magnetic field in the charge pad, shown in the Figure 2.3 (a) and b. The ferrite base has the capability to decrease leakage flux, and results in an increase in the primary-secondary mutual inductance. In a single-sided circular charge pad, the fundamental flux path height is roughly proportional to one quarter of pad diameter whereas P_z is the fundamental flux path height, and P_d is the pad diameter (Mickel et al., 2010)

$$\Delta P_z \propto \frac{1}{4} \Delta P_d \tag{2.1}$$

This means that the pad diameter must increase by four times the increase in the air gap, hence results in large and heavy circular charge pads, making them impractical for systems with large air gaps.

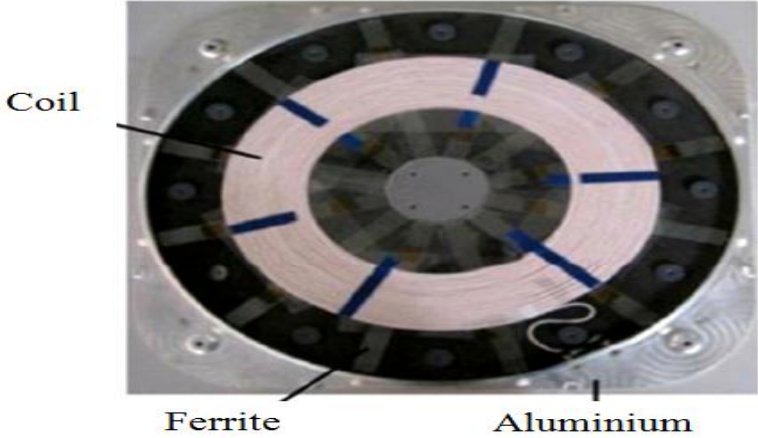


Figure 2.3: Ferrite base

- ***Flux Pipe Charge Pad***

The circular pad with 700mm diameter possesses a coupling co-efficient of 0.2 and is connected with a 175mm air-gap. In order to perform very well, the circular pad diameter needs to be made large, to get a good coupling with larger air-gap. In order to obtain better coupling, a flux pipe coupler was introduced. A final try-to increase/get better (coupling) while it's capability of throwing-flux to "pick-up pad around twice as linked to (circular-topology). It undergoes since substantial efficiency fall, usage of Aluminum as a shield, flux behind the pads to avoid the (eddy current loss in EV Chassis) (Kafeel et al., 2015).

This is also called solenoid coil charge pad, and also contains one or two coils; I core type bar ferrite, and a polarized coupler. In a solenoid coil charge pad, the fundamental flux path height is roughly proportional to one half of pad diameter (Mickel et al., 2010)

$$\Delta P_z \propto \frac{1}{2} \Delta P_l \tag{2.2}$$

Where P_z is called the fundamental flux, and P_l is denoted by pad length, other words pad diameter must increase by two times. It results in increase in the air gap and main enhancement from the circular charge pad. One of the main disadvantages is that it produces double sided magnetic flux distribution.

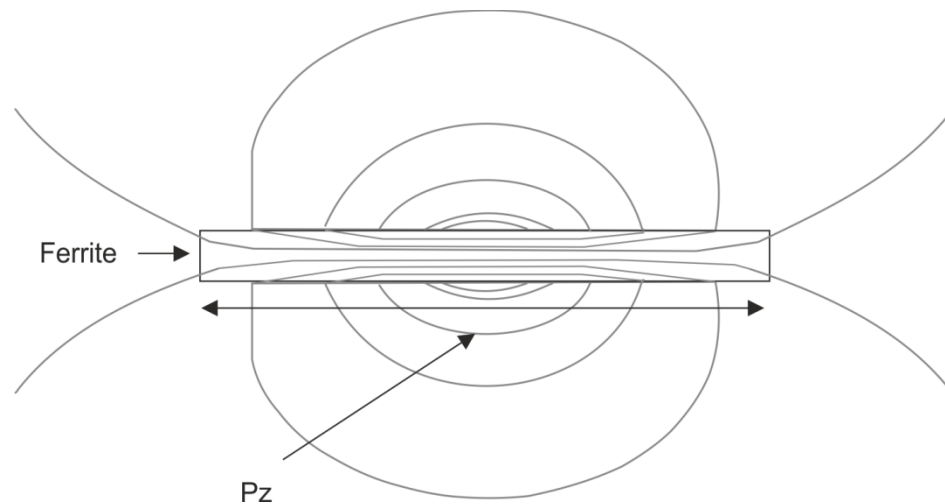


Figure 2.4: Flux Pipe charge pad flux distribution

- ***Double-D Charge Pad***

Double-D (DD) charge pad, is a polarized pad having both of the advantages of circular and flux pipe designs, and is shown in the figure. The two coils of the DD charge pad are magnetically in series, due to such arrangement of windings produces parallel type flux. The two D coils can be wound electrically in series/ parallel, using the same Litz wire. The DD structure has a flux pipe in the center, is made long and remaining length of the coil is reduced to save copper, and lower the AC resistive losses. The magnetic flux distribution of the DD charge pad is same as flux pipe charge pad, of with the important thing that it is single sided (Mickel et al., 2013).

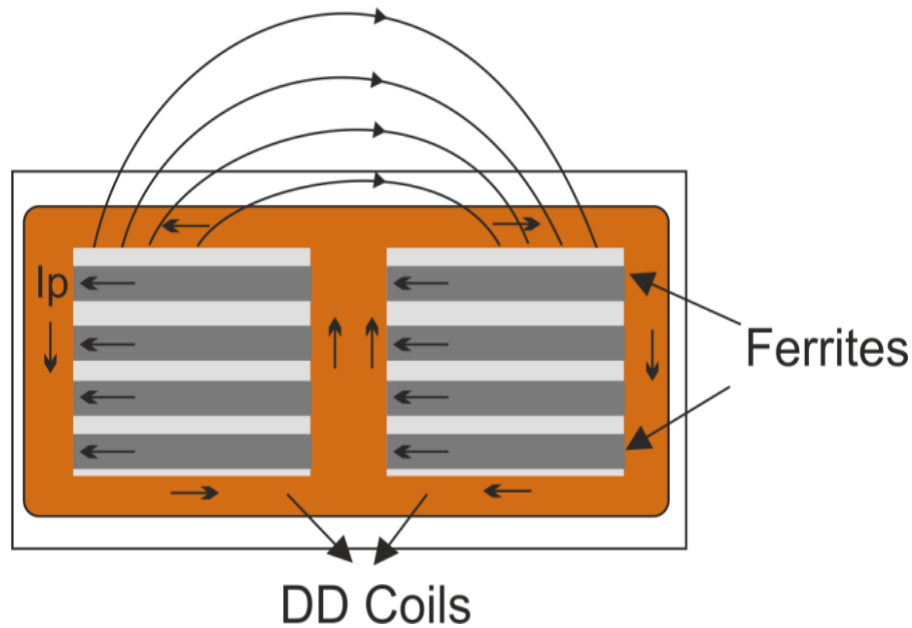


Figure 2.5: DD charge pad flux distribution

- ***Double-D Quadrature Charge Pad***

The Double-D Charge quadrature (DDQ) Pad, as the name shows is a Double-D charge pad with an additional quadrature coil that is spatially decoupled with the DD coil given in the following Figure 2.6. These are designed and used for the receiver system, to enhance misalignment tolerance (Mickel et al., 2013).

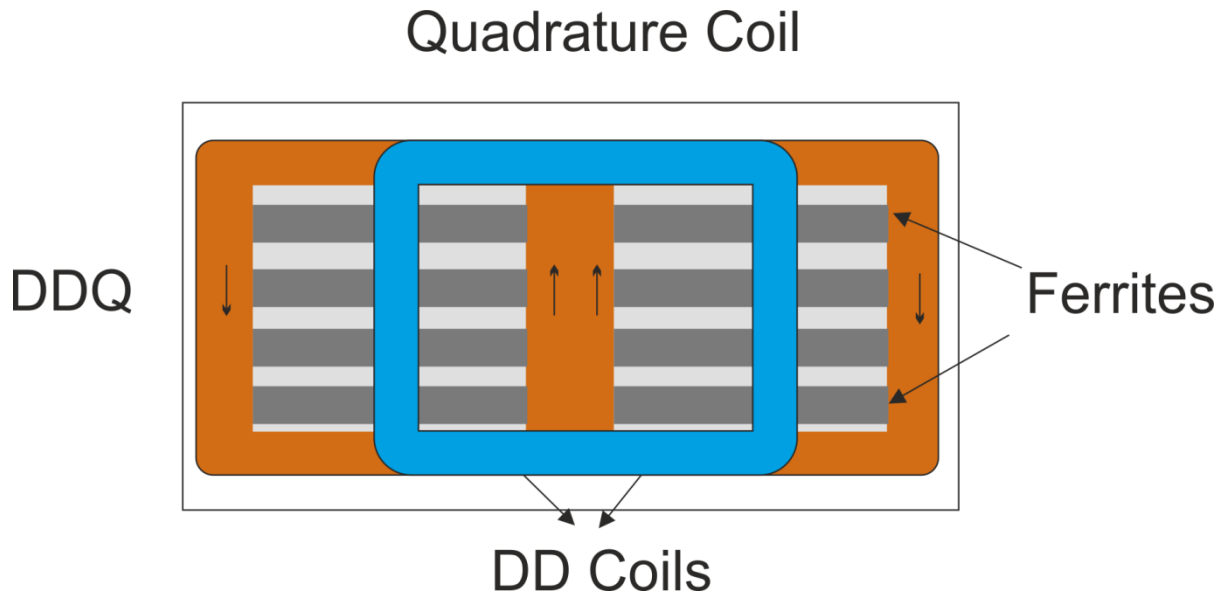


Figure 2.6: DDQ charge pad

2.4. Compensation Topologies

An air cored transformer results in low efficiency, because of large leakage inductances in both primary and secondary windings. There is a smart method to solve the problem presented here, by using capacitors in order to compensate the reactive current. We can use shunt and series compensation in power system, while capacitive compensation is applied to power system for reactive compensation.

1. In the case of shunt compensation, this leads to an increase in power transfer ability and reduction in the reactive voltage drop across line.
2. In case of series compensation, the maximum power transfer capability of the line is better, because of partial compensation of series inductance, and reduction in load angle results enhancement of system stability (Narain et al., 2000).

In order to overcome system losses, capacitors can be connected in series and parallel to both coils. The secondary capacitance is selected as the first step. This is done in such way in order to compensate the secondary leakage inductance, and mutual inductance. This type of compensation leads to the improvement of power transferred to the load.

The primary capacitance is then selected such that, it considers the inductance of the complete circuit. Primary capacitances selected to compensate just the self-inductance of the primary and the inductances of the whole circuit are present. Though, it is a better choice to perform compensation for the entire circuit, so as to the input power factor becomes unity (Narain et al., 2000).

There are two different ways to connect the compensation capacitors are series and parallel to both sides of inductors. Due to these connections there exist 4 different topologies, which are given in the Figures 2.7-2.10.

1. SS (Series-Series)
 2. SP (Series-Parallel)
 3. PS (Parallel-Series)
 4. PP (Parallel-Parallel)
- *SS (Series-Series) Compensation*

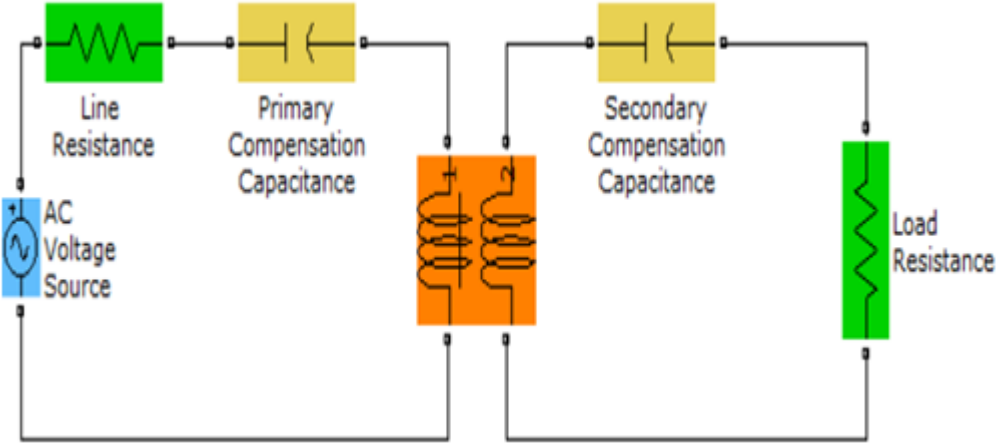


Figure 2.7: Series-series compensation model

The resonant compensation capacitances are

$$C_1 = \frac{1}{\omega_0^2 L_1} \quad (2.3)$$

$$C_1 = \frac{1}{\omega_0^2 L_1} \quad (2.4)$$

The series - series topology works like a “current source” and will produce a constant output current as long as the frequency is high and the load resistance is low enough.

$$I_{\text{LOAD}} = \frac{1}{\omega_0 M} V_1 \quad (2.5)$$

- *SP (Series-Parallel)*

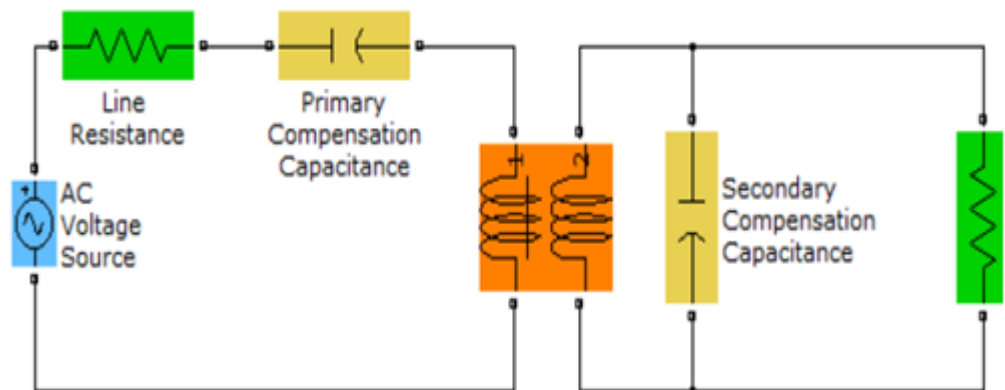


Figure 2.8: Series-parallel topology compensation model

The resonant compensation capacitances of this case are

$$C_1 = \frac{1}{\omega_0^2 \left(L_1 - \frac{M^2}{L_2} \right)} \quad (2.6)$$

$$C_2 = \frac{1}{\omega_0^2 L_2} \quad (2.7)$$

The amplitude of the output voltage can be approximated by

$$V_{\text{LOAD}} = \frac{L_2}{M} V_1 \quad (2.8)$$

- *PS (Parallel-Series)*

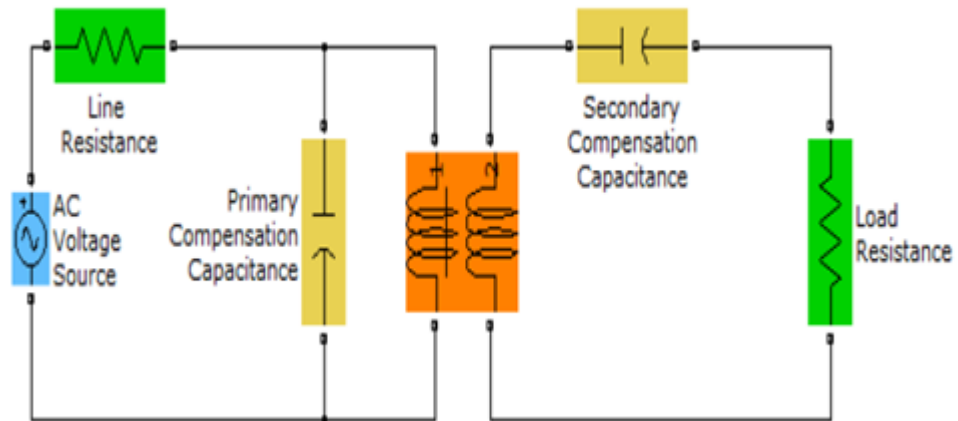


Figure 2.9: Parallel-series compensation model

The resonant compensation capacitances for this type are

$$C_1 = \frac{1}{\omega_0^2 L_1} \quad (2.9)$$

$$C_2 = \frac{1}{\omega_0^2 \left(L_2 - \frac{M^2}{L_1} \right)} \quad (2.10)$$

The amplitude of the output voltage can be approximated by

$$V_{\text{LOAD}} = \frac{M}{L_1} V_1 \quad (2.11)$$

- **PP (Parallel-Parallel)**

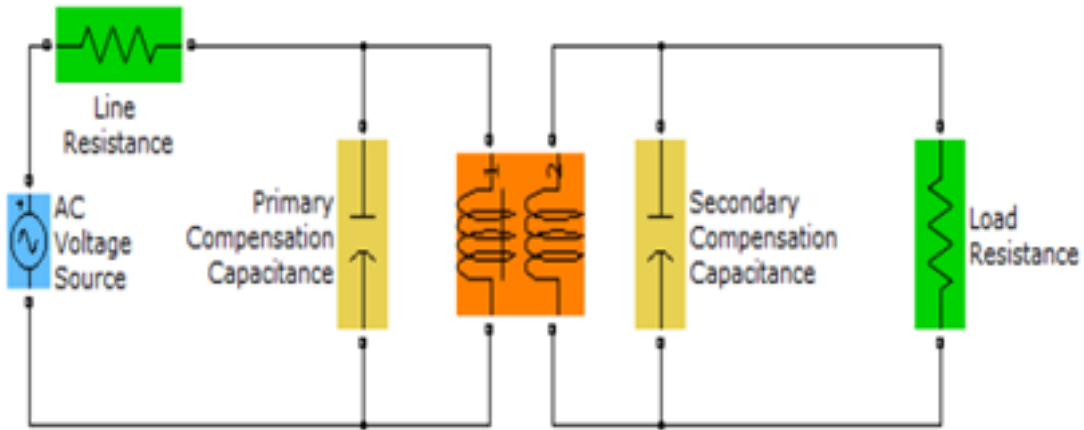


Figure 2.10: Parallel-parallel topology compensation model

The resonant capacitance values are given as

$$C_1 = \frac{1}{\omega_0^2 \left(L_1 - \frac{M^2}{L_2} \right)} \quad (2.12)$$

$$C_2 = \frac{1}{\omega_0^2 \left(L_2 - \frac{M^2}{L_1} \right)} \quad (2.13)$$

Both capacitors have the same values. The parallel-parallel topology acts like a “current source” and will produce a constant output current. The amplitude of the output current can be approximated by the following equation.

$$I_{\text{LOAD}} = \frac{1}{\omega_0 \left(L_1 L_2 - M^2 \right)} V_1 \quad (2.14)$$

Table 2.2: Properties of compensation topologies

Topology	Acts like “sources ”	Independent of “changes”	Power factor small distance	Total impedance at resonant state	Efficiency
SS	<i>Current</i>	C_2	<i>Low/very high</i>	<i>Low</i>	<i>very high</i>
SP	<i>Voltage</i>	C_2	<i>Low/ high</i>	<i>Low</i>	<i>medium</i>
PS	<i>Voltage</i>	C_1	<i>high/ medium</i>	<i>High</i>	<i>medium</i>
PP	<i>Current</i>	C_1	<i>very high/ medium</i>	<i>High</i>	<i>High</i>

2.5. Power Converters and its Control

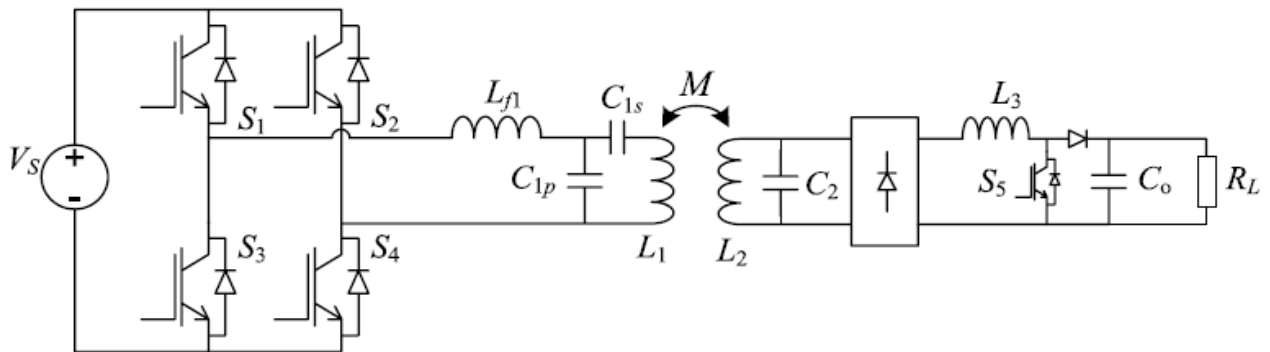


Figure 2.11: Circuit diagram of a typical structure.

IPT systems have primary and secondary side power electronics converters. At the primary side, the main function is to produce high-frequency current in transmitting-coil. Power electronics converter used at the receiving side is a rectifier, which converts the high frequency ac current coming from the primary side into dc current. For the primary side converter, voltage/current source converters are suitable. A full-bridge voltage source resonant converter is the most suitable preference at the transmitting side over a current source converter due to the necessity of a bulky inductor. For a typical design, as in the figure shown above, an LC compensation network is adopted. This ensures the flow of a constant high frequency current in the inductor L_1 . As the reactive power on L_1 needs also to be compensated, an additional capacitor is therefore introduced, that is C_{1s} , and this aids in compensating portion (reactive power) at L_1 . Therefore power rating of L_{f1} is lowered significantly. On the other hand at the secondary side, the type or form of compensation adopted is parallel. Thus with continuous primary coil as a result depicts current-source. In order to also make the current in L_3 to be virtually continuous, and altering duty ratio through switch S_5 , hence output power can be controlled successfully. But in order to control the transfer of power, many different methods can be used, depending on, where the power applied or implemented. In order to control at the secondary side, a boost converter is used. It is introduced after the rectifier, for control purposes due to parallel compensation. If series compensation is used, a buck converter will be more appropriate. It would be necessary to

introduce an additional dc inductor and a diode after the rectifier. Only when it is before the rectifier can the two components be avoided. This may reduce complexity and cost, but the efficiency may decrease a bit (Siqi et al., 2015).

CHAPTER 3

PRINCIPLES OF INDUCTIVE POWER TRANSFER

3.1. Inductive Power Transfer

In Inductive Power Transfer (IPT) systems, power is transferred from one coil to another, through electromagnetic induction. They are similar to well-known magnetically coupled systems such as transformers. However, the air gap is large compared to transformer. Transformer windings are wound on the same core so that coupling is nearly perfect. In the IPT systems, on the other hand, there is no common core and there is a large air gap, resulting in a loose coupling. The efficiency of the loosely coupled systems decreases as the air gap between the primary and secondary coils increases. In order to increase the power transfer capacity, windings are brought into resonance by adding capacitors to the windings. This is called compensation. The LC circuits are operated at resonant frequency. The resonance phenomena enable “effective energy transfer” at the resonant frequency. The compensation system shown in Figure 3.1, for instance, uses a series connected capacitor on each side of the coil system. That is why it is called series-series compensation.

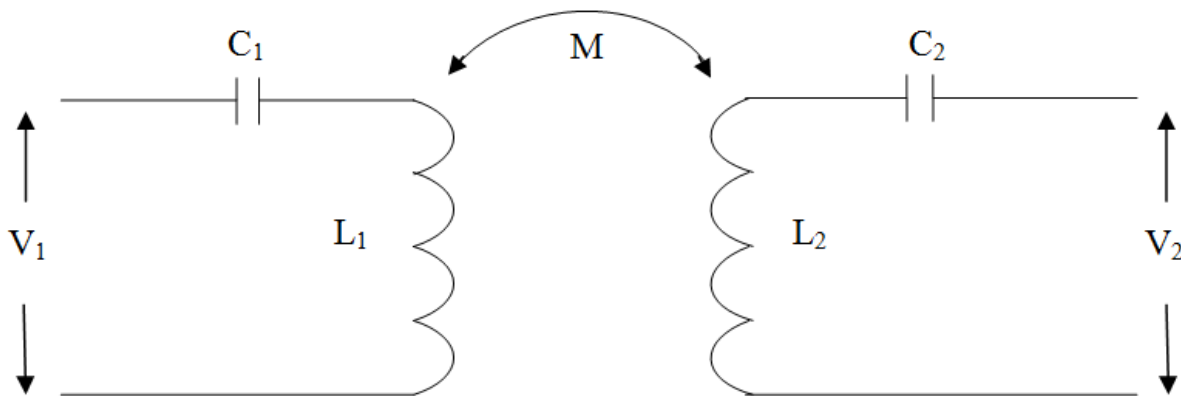


Figure 3.1: Series-Series compensated ICPT circuit

ICPT, being able to transfer a high amount of energy, provides a rapid charging process in many applications. Both static and dynamic charging is possible with IPT. In static charging, the vehicle to be charged carries the secondary side coil and park above the primary coil to start the process. In the dynamic charging systems, vehicles are charged as they move over a track which serves as the primary coil. These vehicles are also called Online Electric Vehicles (OLEV). IPT systems are clean and safe since the power is transferred without any physical contact. They can be used in extreme weather conditions like rain, snow etc. (Kunwar et al., 2014).

3.2. Principle of Operation

If the primary coil is connected to an alternating current source, an alternating current flows through the primary current. This current generates the flux which, in turn, induces ac voltages on the secondary coil, causing power transfer. The principle of IPT system is based on phenomena called mutual induction. The power transferred by two mutually coupled coils with air as it surrounding, and core as a medium is shown in the Figure 3.2.

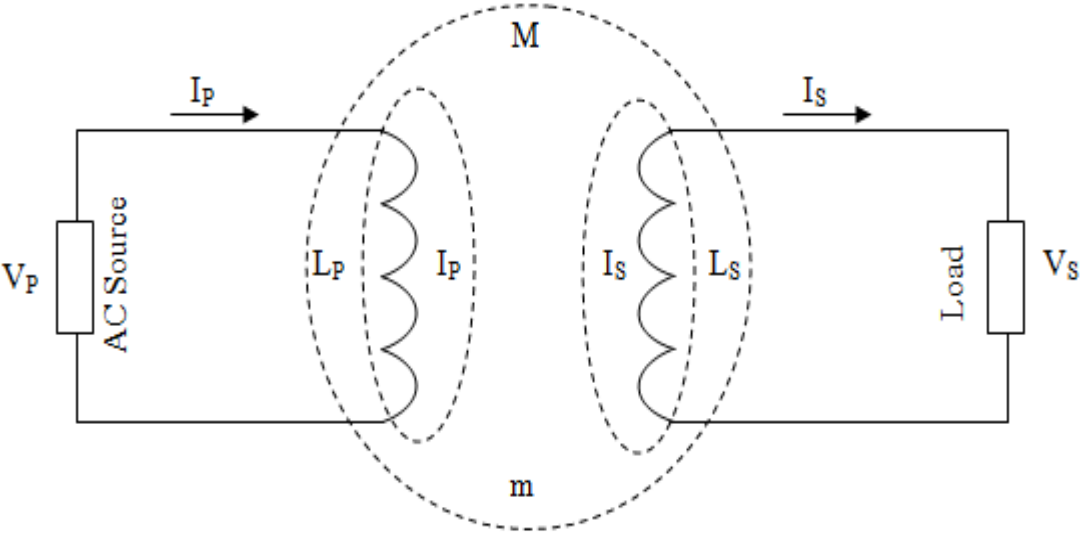


Figure 3.2: Two uncompensated mutually-coupled air cored coils

The subscripts p , s and m represent primary, secondary and mutual while φ_p , φ_s and φ_m represent, respectively, primary leakage flux, secondary leakage flux and mutual flux (Chwei et al.,2005).

The coupling factor of these coils is defined as

$$k = \frac{M}{L_p L_s} \quad 0 \leq k \leq 1 \quad (3.1)$$

This coefficient is a good indication of the quality of the coupling and thus, of power transfer. Mutual inductance, on the other hand, depends on the relative positions and the distance between the coils. If $M = 0$ then there is no coupling between the coils and $k = 0$. Systems are classified as loosely coupled systems if $k < 0.5$ and closely or tightly coupled system if $k > 0.5$. Electrical equivalent circuit of uncompensated mutually coupled coils is given in Figure 3.3.

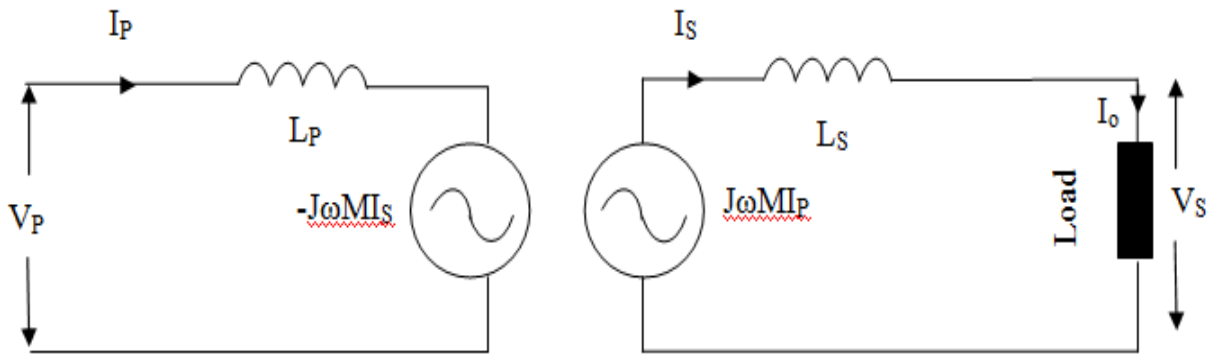


Figure 3.3: Electrical equivalent circuit of uncompensated coils

The performance of an inductive power transfer system is measured by two parameters:

- Open circuit voltage induced across the secondary coil due to the primary current.
- Short circuit current which is the maximum current that this open circuit voltage can force through the winding

The open circuit (V_{OC}) voltage of the secondary coil is equal to the voltage induced across the secondary coil and it can be found by applying Faraday's Law:

$$V_s^{ind} = j\omega M I_p \quad (3.2)$$

If the secondary coil is shorted, the short circuit current of the coil is calculated as follows:

$$I_{sc} = \frac{V_{OC}}{j\omega L_s} = \frac{j\omega M I_p}{j\omega L_s} \quad (3.3)$$

The power that is received from an uncompensated winding is

$$P = \frac{R V_{OC}^2}{R^2 + (\omega L_s)^2} \quad (3.4)$$

The maximum value of the active power that can be transferred to the load is obtained when the load resistance is equal to the winding impedance.

$$R = \omega L_s \quad (3.5)$$

Then, the maximum power is

$$P_{max} = \frac{V_{OC}^2}{2\omega L_s} \quad (3.6)$$

This power can also be specified by the following equation (Kunwar et al., 2014)

$$P_{max} = \frac{|V_{oc}| |I_{sc}|}{2} = \frac{1}{2} \frac{\omega M^2 I_p^2}{L_s} \quad (3.7)$$

If the desired value of the power to be transferred is higher than this maximum value, then the secondary coil has to be compensated. In a compensated system reactive components cancel each other. Then the transferred power is

$$P_{max} = \frac{V_{OC}^2}{R} = \frac{(\omega MI_p)^2}{R} \quad (3.8)$$

By multiplying and dividing this equation by L_s

$$P_{max} = \frac{(\omega MI_p)^2 L_s}{R L_s} \quad (3.9)$$

Quality factor is defined as the ratio of the reactive power of a circuit to its active power, and is an important parameter in power transfer capability.

$$Q_s = \frac{\omega L_s}{R} \quad (3.10)$$

By inserting this into Equation 3.9 the maximum power that can be transferred in a compensated system can be expressed as follows:

$$P_{max} = \frac{\omega M^2 Q_s I_p^2}{L_s} \quad (3.11)$$

3.3. Need of High Frequency

From Equation (3.11) it is obvious that, in order to increase the power transfer capacity, ωI_p should be maximized, since the other parameters are fixed. Also, primary current is kept at its rated value to utilize the coil in its highest capacity. What is left is the frequency. For fixed primary current, mutual inductance and self-inductance values power transfer capacity is directly proportional with the frequency.

Operation frequencies of today's power electronic converters are between 10 kHz and 100 kHz for power levels in the kW ranges. In this frequency range typical choice of core material is ferrites and, Litz wires are used to avoid the negative impacts of skin effect. The following subsections related to the discussion of the choice of material for coil, and core (Kunwar et al., 2014).

3.3.1. Material selection for coil

Current density distribution is constant, over the whole cross sectional area of conductor (in case of dc current). Furthermore as the frequency increases, current flows through the surface of conductor in place of entire cross sectional area of conductor. This effect is known as "skin effect", due to which effective resistance increases. The distance δ called skin depth. The skin depth for a round conductor is given by equation which is given below (Albert et al., 2012)

$$\delta = \frac{1}{\sqrt{\pi f \mu_0}} \quad (3.12)$$

Frequency of the current, permeability, and conductivity of material are denoted by f , μ and ρ Proximity effect is another negative impact of high frequency which increases the effective resistance. Proximity and skin effects create extra losses in coil windings due to this high resistance. Current density distributions at dc, 60 Hz and 200 kHz are shown in Figure 3.4. These results are obtained by FEMM software for a copper wire.

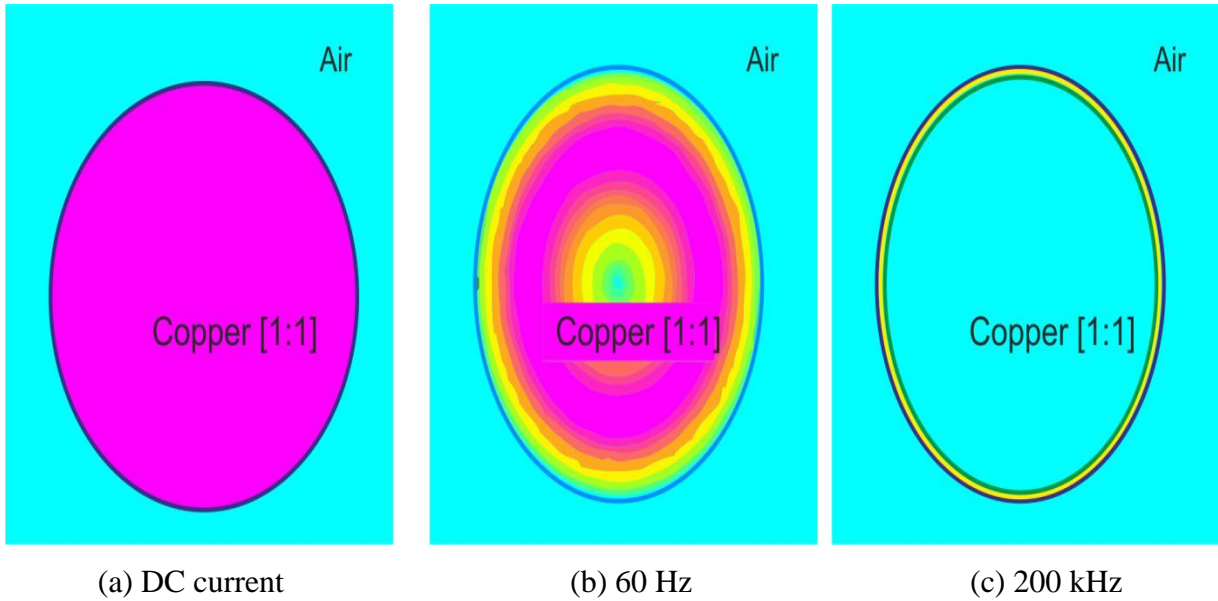


Figure 3.4: Current density distributions in copper wire

Pink color represents the current density. In the case of dc current it is uniform across the whole cross section. As the frequency increases it becomes non uniform and concentrates around the circumference. Litz wire is used to reduce the effective ac resistance (Kunwar et al., 2014).

3.3.2. Material selection for core

Coils of IPT systems may be designed to have a core or without a core. Of course, coreless systems are lighter and cheaper. However, the coupling is not good and efficiency is reduced.

As the frequency increases core losses increase too and linear relationship between power and frequency may be lost due to saturation. They increase the eddy current losses in the conducting material too. Also, when cores are used, the system becomes heavier and more expensive. On the positive side of using cores, leakage inductance decreases and more power can be transferred. Also, cores act like magnetic shields so that the flux does not stray around, reducing the possibility of harm to environment (Kunwar et al., 2014).

3.4. Field Shaping Techniques

Leakage flux in loosely coupled IPT systems is large and therefore minimization of leakage is vital for efficiency. There are some techniques to shape the flux so that leakage is reduced, and the flux distribution around a wire when there is no shaping technique is used.

Flux can be directed by using some conductive metals. A good conductor with a very low magnetic permeability such as copper or aluminum can be used for this purpose. At the presence of time varying flux, eddy currents are induced in these materials, creating in turn, their own magnetic flux lines in the opposite direction. Finally it has been concluded that use of field shaping techniques provides better efficiency, also reduces leakage flux. it is preferable as compare to without field shaping techniques. As a result, the flux lines interact and the external flux bends instead of entering the copper material.

3.5. Compensation Systems

It has been proven above that the secondary coil needs to be compensated if it is desired to transfer more power to the load.

In the primary side also compensation is necessary to increase the input power factor. In IPT systems, due to leakage and magnetic inductances, and range of operating frequency (10 kHz to 100 KHz) the system is highly inductive and power factor is poor. Poor power factors result in increased system losses.

As the system is inductive on both sides, capacitors are used to compensate the coils. Capacitors can be connected in series or in parallel with the coils. As a result, there exist 4 different topologies, which are given in the Figure 3.7 (Kunwar et al., 2014).

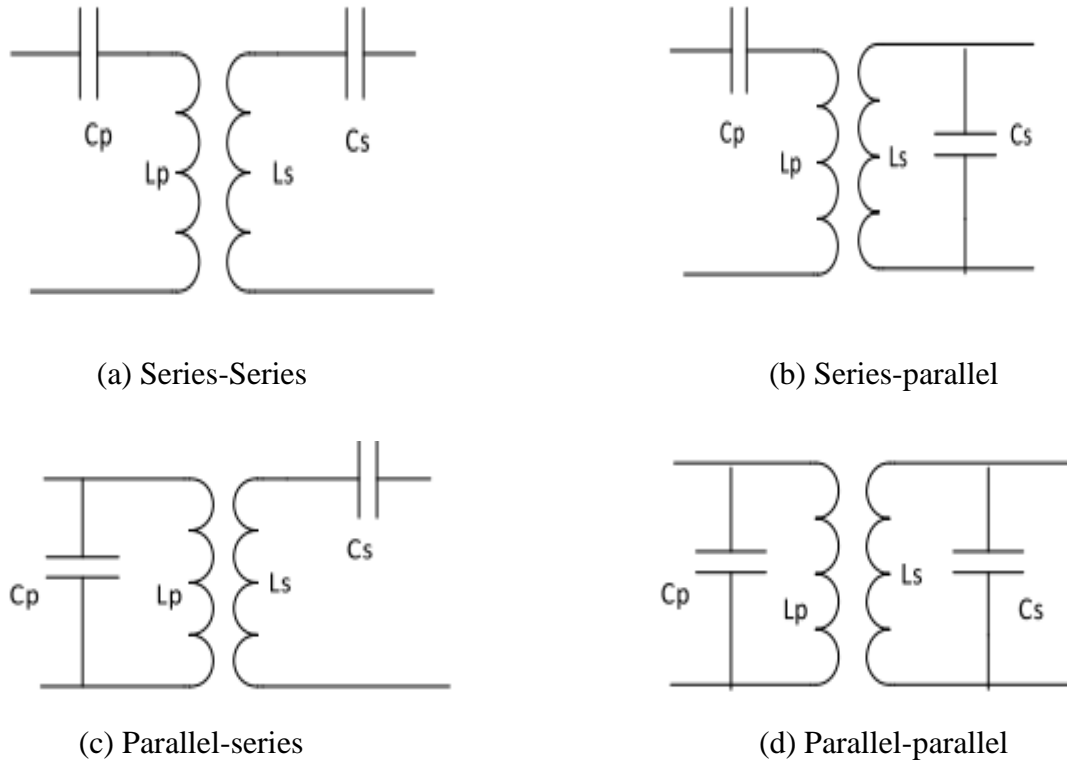


Figure 3.5: Basic compensation topologies

When series compensation is used in the primary, it should be supplied by a voltage source since it requires a high voltage. When parallel compensation is used the input should be a current source. The function of the primary capacitance is to cancel the reactive component of the input impedance. The secondary side capacitor is chosen to bring the secondary in resonance so that maximum power is transferred.

When designing a compensation circuit the first step is to calculate the secondary side capacitor. For all topologies, the value of the capacitor that would compensate the self-inductance of the secondary coil is calculated as

$$C_s = \frac{1}{\omega_o L_s} \quad (3.13)$$

Here, ω_o is the operating frequency (resonance frequency) of the system. Similarly, primary capacitance is calculated to bring the power factor to unity. Table 3.1 shows the formulas to

use in the calculation of capacitors for all four topologies. Also shown in the table are the primary and secondary quality factors (Q_p, Q_s) defined at the resonant frequency (ω_o).

In literature, there are many examples in which primary capacitances have been chosen to compensate just the self-inductance of the primary (Albert et al., 1991).

As seen from the table, primary capacitance value required for compensation in the SS topology is independent of the coupling.

Consider the following circuit in Figure 3.8, in order to understand how secondary compensation improves power transfer.

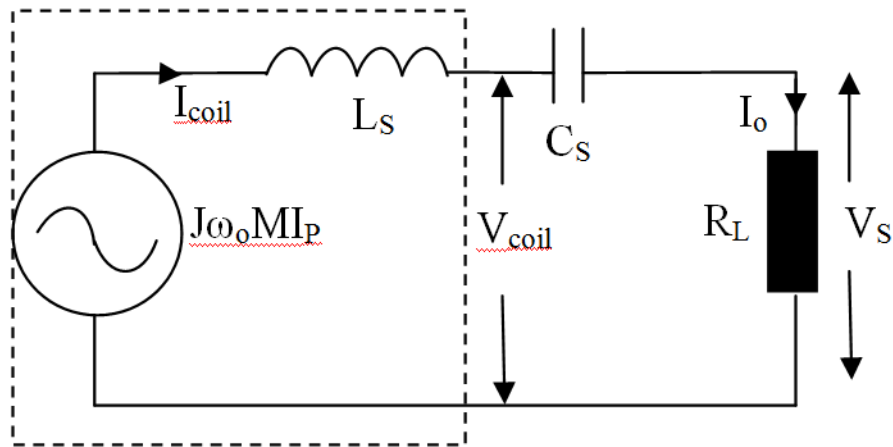


Figure 3.6: Series compensated secondary

For maximum power transfer VA rating of coil is represented in mathematical form given below

$$VA = V_{coil} \times I_{coil} \quad (3.14)$$

Where

$$V_{coil} = \frac{j\omega M I_p}{R_L} \left(R_L + \frac{1}{j\omega_o C_s} \right)$$

$$I_{coil} = \frac{j\omega MI_p}{R_L}$$

Equation (3.13) can be expressed in terms of the quality factor as follows:

$$VA = |V_{oc}||I_{sc}| \frac{\omega_o L_s}{R_L} (1 - j \frac{\omega_o L_s}{R_L}) \quad (3.15)$$

The V_{oc} , and I_{sc} have been defined earlier. The real part of the equation show the active power transferred to the load and the imaginary component shows the reactive power that needs to be supplied by the coil. Table 3.2 gives the VA rating, active power and reactive power for an uncompensated system, for a series compensated secondary and a parallel compensated secondary for a resistive load (Kunwar et al., 2014).

Table 3.1: Secondary coil ratings for maximum power transfer to load (Kunwar et al., 2014)

Coil parameters	Uncompensated	Series compensated	Parallel compensated
VA rating	$\frac{ V_{oc} I_{sc} }{2}$	$ V_{oc} I_{sc} (1 - jQ_s)Q_s$	$ V_{oc} I_{sc} (1 - jQ_s)Q_s$
Real power	$\frac{ V_{oc} I_{sc} }{2}$	$ V_{oc} I_{sc} Q_s$	$ V_{oc} I_{sc} Q_s$
Reactive power	0	$-j V_{oc} I_{sc} Q_s^2$	$-j V_{oc} I_{sc} Q_s^2$

It can be concluded that for compensated coil, maximum power transfer capability increases to $2Q_s$ and VA rating increases to $Q_s \times \sqrt{1+Q_s^2}$ when the secondary side is compensated. Following equations show the reflected values of the resistance from the secondary to the primary for different compensation topologies.

$$R_{r_{ss}} = R_{r_{ps}} = \frac{\omega_o M^2}{R_L}$$

$$R_{r_sp} = R_{r_pp} = \frac{M^2 R_L}{L_s^2}$$

When the coupling decreases reflected resistance also decreases. If the primary side compensation is series, this causes in increased current and therefore more power can be transferred. If the primary side compensation is parallel, the source is current type and reduced resistance means reduced power (Chwei et al.,2000).

All the basic four topologies have different advantages and drawbacks. Selection of topology depends on the application. In battery charging applications constant voltage and constant current are required and compensation topology needs to provide this feature. In dynamic charging systems, primary coil is actually a long wire, causing in high leakage reactance and voltage drop. Therefore, series compensation is more advantageous for these systems since they can provide the high voltage required to compensate this voltage drop. If constant voltage is required at the secondary series compensation, if constant current is required parallel compensation is preferred. At the other hand primary side series capacitors are used to reduce primary voltage and primary side parallel capacitors are used to provide large primary current (Kunwar et al., 2014).

CHAPTER 4

COIL DESIGN

IPT system design is a complicated process. Although there are some papers describing design methodologies, there is not a generally accepted design process yet. Several studies have been carried out in order to select the most appropriate compensation topology for ICPT systems, depending on the application and taking into account the stability of the configuration (Yuan et al., 2007). However, these studies do not include a general design procedure to select the optimal number of coils and sections of the windings for a desired transferred power. Two design procedures are presented, but there still remain many design decisions that depend on the actual case and the experience of the designer (Byung et al., 2005).

An optimum design methodology that seems to be working well is given in (Sallan et al., 2009). The method described in this paper is an iterative one which yields a possible solution at each step. Then the optimum solution is found among the set of solutions. The logic behind this method and its steps are explained in this chapter.

The methodology given in (Sallan et al., 2009) is based on the algorithm given in Figure 4.1. It starts with the selection of coil geometry, maximum current density for the coils, and maximum number of turns allowed. In the iteration process first the number of turns for each coil is assumed to be one and some initial values are assigned to coil cross-section areas. Also, a frequency factor which determines the operation frequency is started at one.

In the first step inductance values are calculated for the given initial values. Based on these values current, voltage, power values and quality factors are calculated for the compensation topology of choice. If the load power is less than the targeted value frequency is increased and calculations are repeated for the same coil size. This iteration is repeated until the desired power level is reached. Once the power level is reached the current density values of the coils are checked to see if this is an acceptable operation point. If the current density is above the defined limit at a coil, corresponding cross-section area is increased and the iteration is repeated.

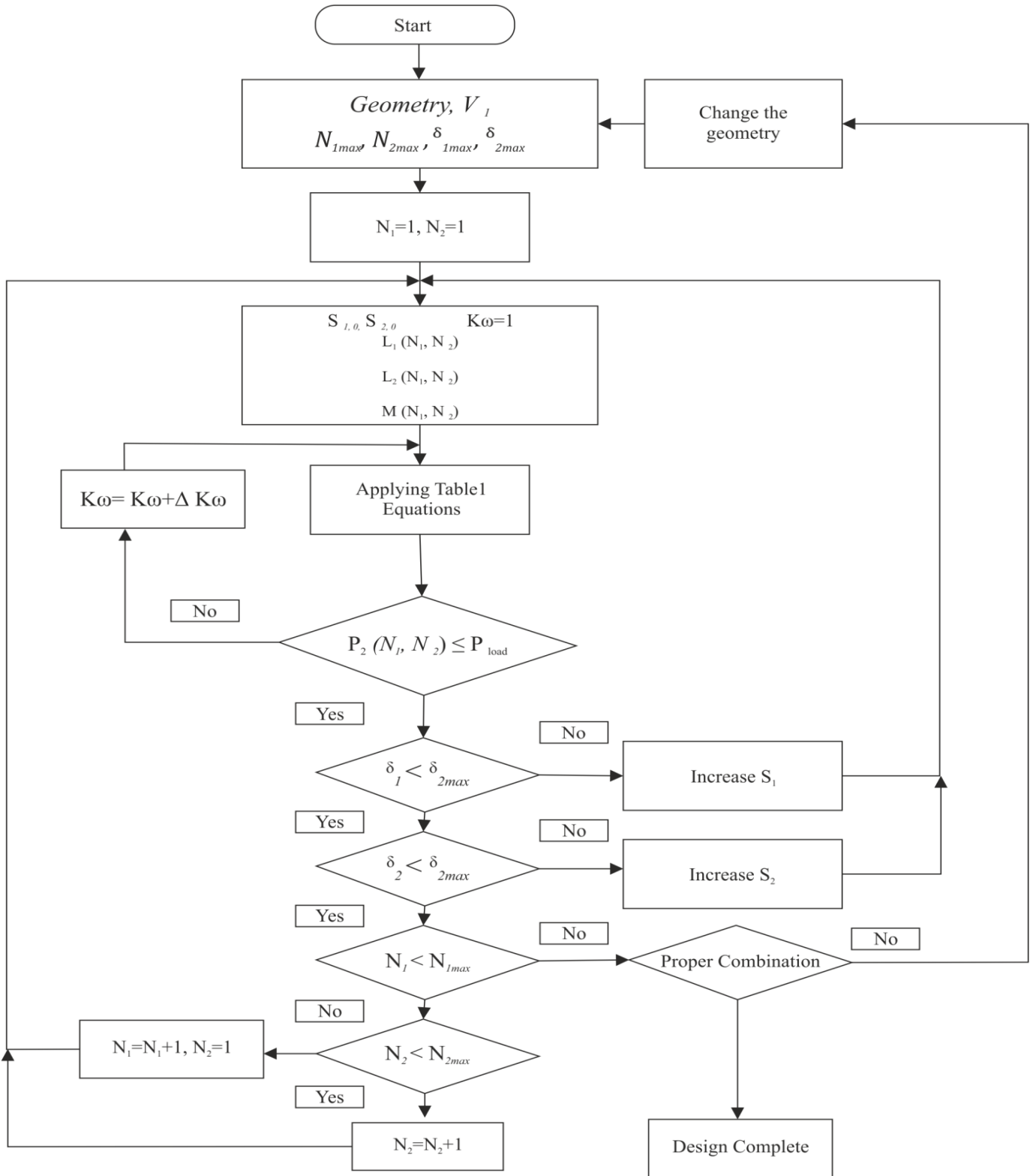


Figure 4.1: The flowchart for IPT system design proposed in (Sallan et al., 2009)

4.1. Design Methodology

To design an ICPT system, following parameters are required:

- Winding dimensions
- Maximum operating frequencies (ω_0)
- Supply voltage value and
- Power value to be transferred to the load (P_{Load})
- Voltage value required by the load (V_{Load}).

For the purpose of simplicity, it could be assumed that the load is a resistor which absorbs a power value P_{Load} of at a voltage of V_{Load} . In that case the equivalent value of the load resistor is

$$R_L = V_{Load}^2 / P_{Load} \quad (4.1)$$

The desired power and voltage can be obtained with any number of turns per coil. Since the input current is $I_1 = V_1 / Z_1$ for the system, the same result can be obtained by low currents and high impedance (high frequency) or high current at low impedance (low frequency).

Active power that is transferred to a load in a compensated system was calculated in Chapter 3 and is repeated here:

$$P_{max} = \frac{\omega M^2 Q_s I_p^2}{L_s} \quad (4.2)$$

As mentioned earlier, transferred power depend on the M^2 / L_s ratio. In order to increase this ratio a large mutual inductance is desired which required the use of ferrite cores to increase the coupling factor. However, this also results in higher core losses, nonlinearity and a heavy system. Therefore, a coreless design is proposed in the paper. It is suggested that with a proper compensation, efficiency above 95% is possible at low resonance frequencies.

The first step in the design is the selection of core geometry. Cores could be circular or rectangular. While circular cores are easier to build and have better coupling, rectangular cores have the advantage of having a better tolerance to misalignment.

Once the core geometry is selected, self-inductance and mutual inductance values can be calculated. The equations used for this purpose are given in the appendix for both geometries.

Results of inductance calculations are used to find the current and power values. First the capacitor value to compensate the secondary coil is calculated as

$$C_s = \frac{1}{\omega_o L_s} \quad (4.3)$$

Then, the primary side compensation capacitor and quality factors are determined based on the compensation topology by using the equations given in Table 4.1.

Table 4.1: Compensation capacitance values for all classical topologies

Topologies	Primary Capacitance (C_1)	Primary quality factor (Q_p)	Secondary quality factor (Q_s)
SS	$\frac{L_s C_s}{L_p}$	$\frac{R_L L_p}{\omega_o M^2}$	$\frac{\omega_o L_s}{R_L}$
SP	$\frac{L_s C_s}{L_p} \frac{1}{(1 - k^2)}$	$\frac{\omega_o L_p L_s^2}{M^2 R_L}$	$\frac{R_L}{\omega_o L_s}$
PS	$\frac{L_s C_s}{L_p} \frac{1}{Q_s^2 k^4 + 1}$	$\frac{R_L L_p}{\omega_o M^2}$	$\frac{\omega_o L_s}{R_L}$
PP	$\frac{L_s C_s}{L_p} \frac{1 - k^2}{Q_s^2 k^4 + (1 - k^2)^2}$	$\frac{\omega_o L_p L_s^2}{M^2 R_L}$	$\frac{R_L}{\omega_o L_s}$

It is obvious that these parameters depend on the frequency. Therefore, an initial value and a maximum value are determined for the frequency. The maximum value is chosen as 20 kHz in the paper. The next step is to calculate the currents, voltages and power values. This requires the calculation of equivalent impedance values seen between the input terminals. These impedance equations are given between (4.4) and (4.7) for each compensation topology.

$$\bar{Z}_{T_{SS}} = (R_1 + j(L_1\omega - 1/C_1\omega)) + \omega^2 M^2 / (R_2 + R_L + j(L_2\omega - 1/C_2\omega)) \quad (4.4)$$

$$\bar{Z}_{T_{SP}} = (R_1 + j(L_1\omega - 1/C_1\omega)) + \omega^2 M^2 / (R_2 + jL_2\omega + R_L / 1 + jR_L C_2\omega) \quad (4.5)$$

$$\bar{Z}_{T_{PS}} = 1 / (R_1 + jL_1\omega) + \omega^2 M^2 / (R_2 + R_L + j(L_2\omega - 1/C_2\omega)) + jC_1\omega \quad (4.6)$$

$$\bar{Z}_{T_{PP}} = 1 / 1 / (R_1 + jL_1\omega) + \omega^2 M^2 (1 + jR_L C_2\omega) / (R_L + (R_2 + jL_2\omega)(1 + jR_L C_2\omega)) + jC_1\omega \quad (4.7)$$

Then I_1 is found from $I_1 = V_1/Z_T$ and all other values are calculated from the equations given in Table 4.2. Note that all currents and voltages are in phasor form.

Table 4.2: Equations to calculate the electrical quantities for each compensation topology

SERIES-SERIES		SERIES-PARALLEL	PARALLEL-SERIES	PARALLEL-PARALLEL
\bar{I}_p	\bar{I}_1	\bar{I}_1	$\bar{I}_1 - j\omega C_1 \bar{V}_1$	$\bar{I}_1 - j\omega C_1 \bar{V}_1$
\bar{I}_{C1}	\bar{I}_p	\bar{I}_p	$\bar{V}_1 j\omega C_1$	$\bar{V}_1 j\omega C_1$
$\bar{V}C_1$	$\bar{I}_1 / jC_1\omega$	$\bar{I}_1 / jC_1\omega$	\bar{V}_1	\bar{V}_1
\bar{I}_s	$j\omega M \bar{I}_p / (R_2 + R_L + j(L_2\omega - 1/C_2\omega))$	$j\omega M (1 + jR_L C_2\omega) \bar{I}_p / (R_L + (R_2 + jL_2\omega)(1 + jR_L C_2\omega))$	$j\omega M \bar{I}_p / (R_2 + R_L + j(L_2\omega - 1/C_2\omega))$	$j\omega M (1 + jR_L C_2\omega) \bar{I}_p / (R_L + (R_2 + jL_2\omega)(1 + jR_L C_2\omega))$
\bar{I}_2	\bar{I}_s	$1 / (1 + jR_L C_2\omega) \times \bar{I}_s$	\bar{I}_s	$1 / (1 + jR_L C_2\omega) \times \bar{I}_s$
$\bar{I}C_2$	\bar{I}_s	$jR_L C_2 \omega \bar{I}_2$	\bar{I}_s	$jR_L C_2 \omega \bar{I}_2$
$\bar{V}C_2$	$\bar{I}_s / jC_2\omega$	$\bar{I}C_2 / jC_2\omega$	$\bar{I}_s / jC_2\omega$	$\bar{I}C_2 / jC_2\omega$
\bar{V}_L	$R_L \bar{I}_2$	$\bar{V}C_2$	$R_L \bar{I}_2$	$\bar{V}C_2$
Q_p	$L_1 R_L / \omega M^2$	$\omega L_1 L_2^2 / R_L M^2$	$L_1 R_L / \omega M^2$	$\omega L_1 L_2^2 / R_L M^2$
Q_s	$\omega L_2 / R_L$	$R_L / \omega L_2$	$\omega L_2 / R_L$	$R_L / \omega L_2$

The efficiency of the system is given by Equation (4.8).

$$\eta = \frac{R_L I_2^2}{R_1 I_P^2 + R_1 I_S^2 + R_L I_2^2} \quad (4.8)$$

This equation can be expressed as

$$\eta = \frac{R_L}{R_1 \left(\frac{I_P}{I_2}\right)^2 + R_2 \left(\frac{I_S}{I_2}\right)^2 + R_L} \quad (4.9)$$

The ratio of the currents in this equation and corresponding efficiency equations are given in Table 4.3 for each topology.

Table 4.3: The ratio of the currents and efficiencies for each compensation topology

	SERIES-SERIES AND PARALLEL-SERIES	SERIES-PARALLEL AND PARALLEL-PARALLEL
$ I_S / I_2 $	1	$\sqrt{1 + R_L^2 C_2^2 \omega_0^2}$
$ I_P / I_2 $	$(R_2 + R_L) / \omega_0 M$	$\sqrt{\frac{R_2^2 + (L_2 \omega_0 + R_2 R_L C_2 \omega_0)^2}{\omega_0^2 M^2}}$
η	$\frac{R_L}{(R_L + R_2)(1 + R_1 \times (R_2 + R_L / \omega_0^2 M^2))}$	$\frac{R_L}{(R_L + R_2 + \frac{R_2 R_L^2}{\omega_0^2 L_2^2} + \frac{R_1 R_2^2}{\omega_0^2 M^2} + \frac{R_1 L_2^2}{M^2})}$

Therefore, selection of initial frequency is important. It should have a high value so that the frequency dependent terms in the efficiency equation can be neglected. This condition can be met if

$$\omega_0 \gg \sqrt{R_1 \left(\frac{R_2 + R_L}{M}\right)} \quad (4.10)$$

for series compensation on the secondary, and if

$$\omega_0 \gg \sqrt{\frac{R_2 R_L^2 M^2 + R_1 R_2^2 L_2^2}{L_2 M}} \quad (4.11)$$

for parallel compensation on the secondary. If these conditions are met, the corresponding efficiencies would be

$$\eta_{MAX} \cong \frac{R_L}{R_L + R_2} \quad (4.12)$$

for series compensation, and

$$\eta_{MAX} \cong \frac{R_L}{R_L + R_2 + \frac{R_1 L_2^2}{M_2}} \quad (4.13)$$

For parallel secondary compensation now, the operating frequency of the system may be defined by multiplying these minimum frequencies by a frequency factor (K_ω).

For Series- Series compensation the operating frequency then

$$\omega_{OP} = K_\omega \frac{\sqrt{R_1 (R_2 + R_L)}}{M} \quad (4.14)$$

Whereas for the Series-Parallel topology

$$\omega_{OP} = K_\omega \times \frac{\sqrt{R_2 R_L^2 M^2 + R_1 R_2^2 L_2^2}}{L_2 M} \quad (4.15)$$

If, at the end of the first round of calculations the load power is less than the maximum transferrable power, the operation frequency is increased by increasing K_ω in a certain step. This is repeated until the load power reaches up to the maximum amount of power available,

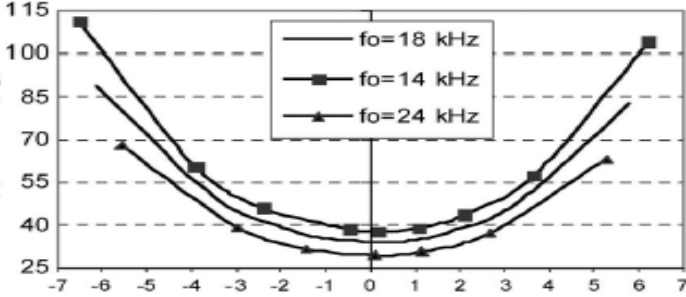


Figure 4.2: Copper-mass vs. $\ln \frac{Q_p}{Q_s}$

as long as the frequency is below the maximum allowed value. These values can be found in different wire sections and for an application with frequency up to 20 kHz, this reference indicates that the appropriate wire gauge is AWG19. When this condition is met, the current densities are checked. Current densities could be between 3 A/mm^2 and 6 A/mm^2 . The authors consider this latter value too high, and they have chosen a limit of 4 A/mm^2 (Sergeant et al., 2008).

If the density is above these limits, the wire cross-section area is increased. Then all inductances should be re-calculated, current and power calculations should be repeated and frequency should be changed until a solution is found again.

This iterative process generates proper K_ω and wire cross-section solutions for each (N_1, N_2) pair. At the end the matrix of solutions would have a dimension of $N_{1max} \times N_{2max}$. An optimum solution is chosen by using the following criteria:

- 1- $P_L(N_1, N_2) = P_{load}$
- 2- $V_L(N_1, N_2) = V_{load}$
- 3- $f_{op}(N_1, N_2) \leq f_{max}$
- 4- $Q_p(N_1, N_2) > Q_s(N_1, N_2)$
- 5- $\delta_1(N_1, N_2) \leq \delta_{1max}(N_1, N_2)$
- 6- $\delta_2(N_1, N_2) \leq \delta_{2max}(N_1, N_2)$

The fourth condition is necessary for a stable operation.

These conditions may be satisfied for more than one pair of turn numbers. In that case the optimal solution is the one that results in less copper use. For a sample design of 200 kW systems, variation of the copper amount in kg against the natural logarithm of quality factor ratio $Ln\left(\frac{Q_p}{Q_s}\right)$ is given as in Figure 4.2. It shows that if Q_p is slightly bigger than Q_s the copper amount is minimum. This result shows that the design is optimal when the absolute value of $\ln\frac{Q_p}{Q_s}$ is minimum, and this fact can be used to define a design coefficient, K_D as given in Equation (4.16)

$$K_D = \frac{1}{1 + \left|Ln\frac{Q_p}{Q_s}\right| + \left|Ln\frac{f_{max}}{f_o}\right|} \quad (4.16)$$

In this equation

f_{op} = optimal resonant frequency

f_{max} = maximum allowable frequency

The value of this parameter varies between 0 and 1. The solution that yields the highest K_D is the optimal solution. Theoretically, $K_D = 1$ if $Q_p = Q_s$ and $f_{op} = f_{max}$.

4.2. Results of MATLAB Code

The iterative technique described above is tested in computer via MATLAB software. Maximum number of turns was defined to be 30 and 10 for the primary and secondary, respectively. For each pair of turn numbers, a solution was found iteratively, starting from an initial cross section are and by changing the frequency. Figures 4.3-4.8 show the results.

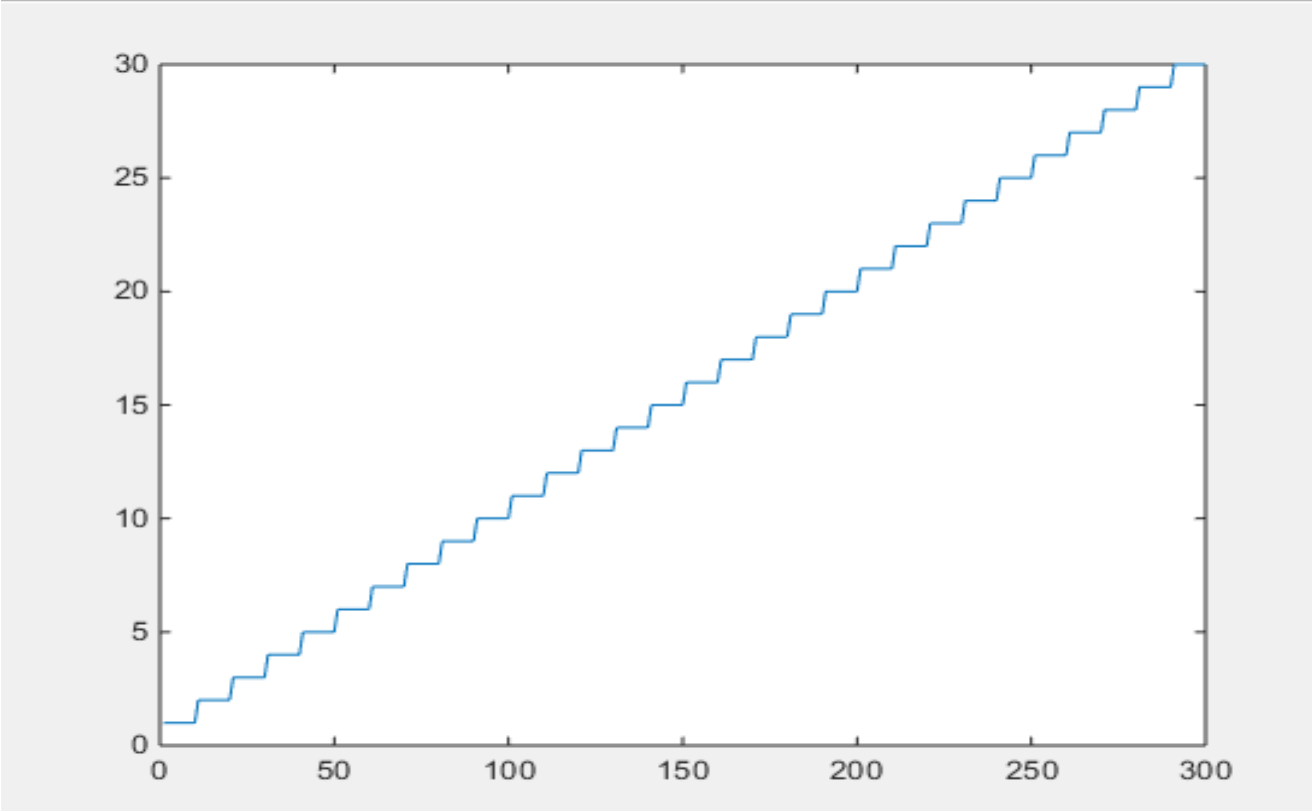


Figure 4.3: Turn number variation for the primary at each step

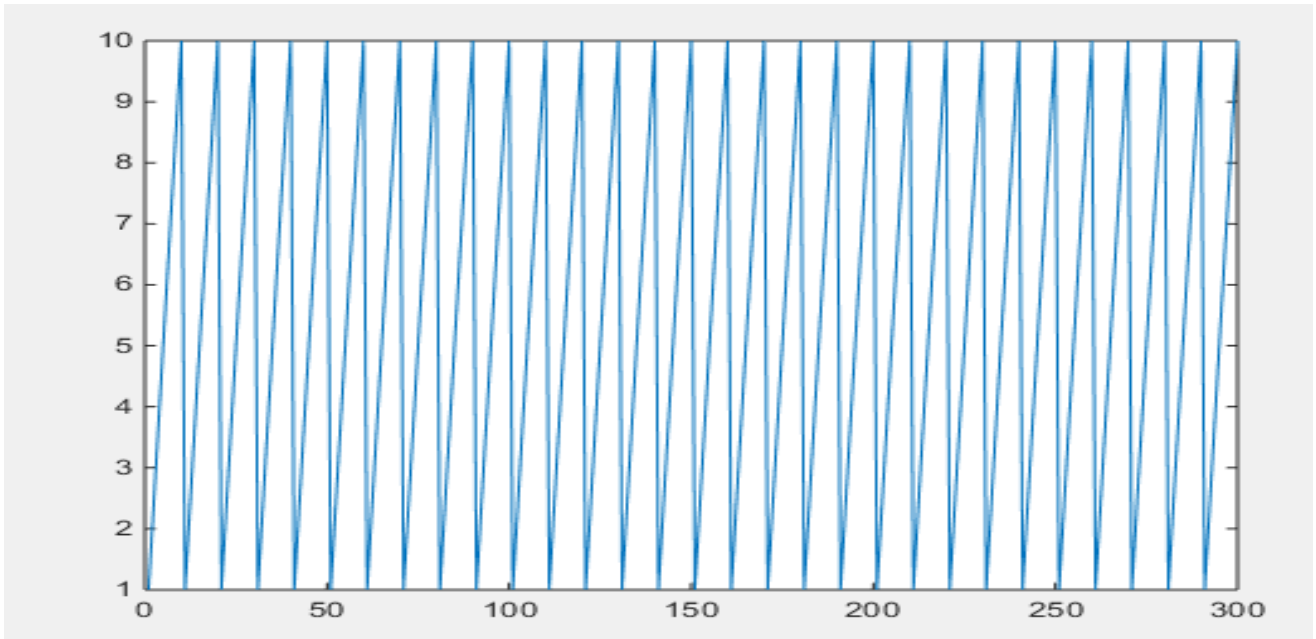


Figure 4.4: Turn number variation for the secondary at each step

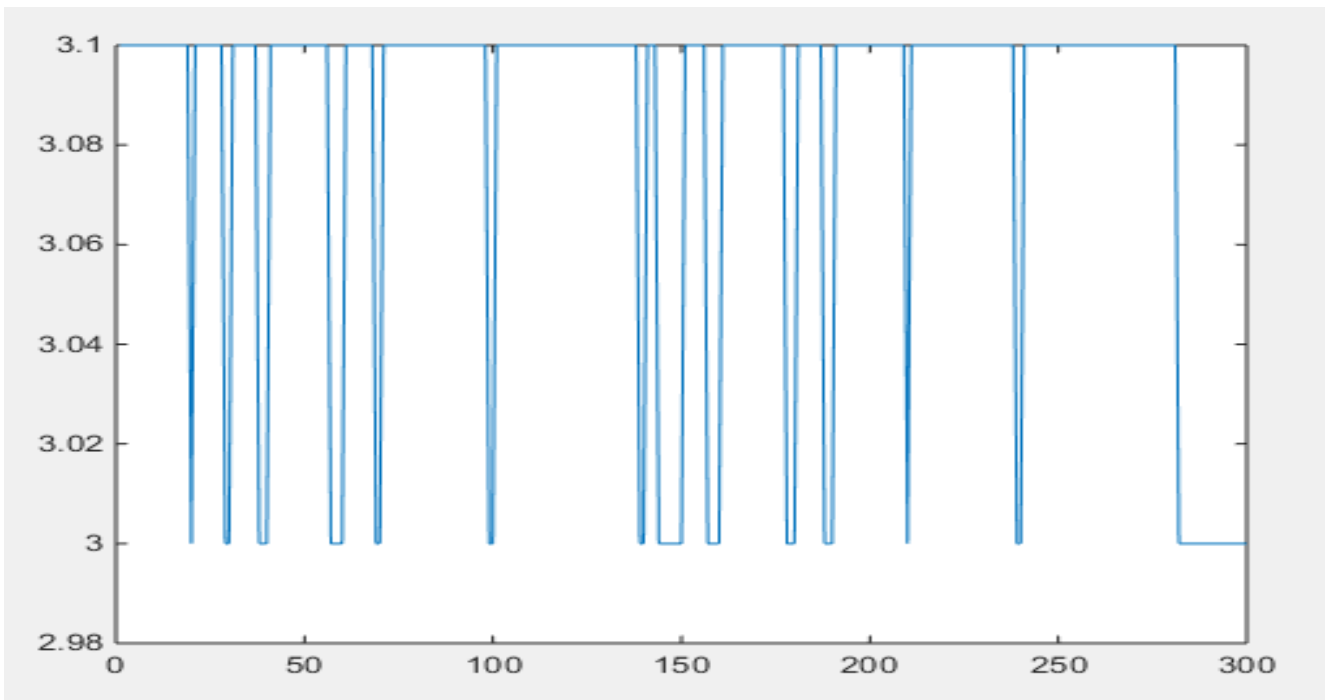


Figure 4.5: Cross-section area variation for the primary for each step (in mm^2)

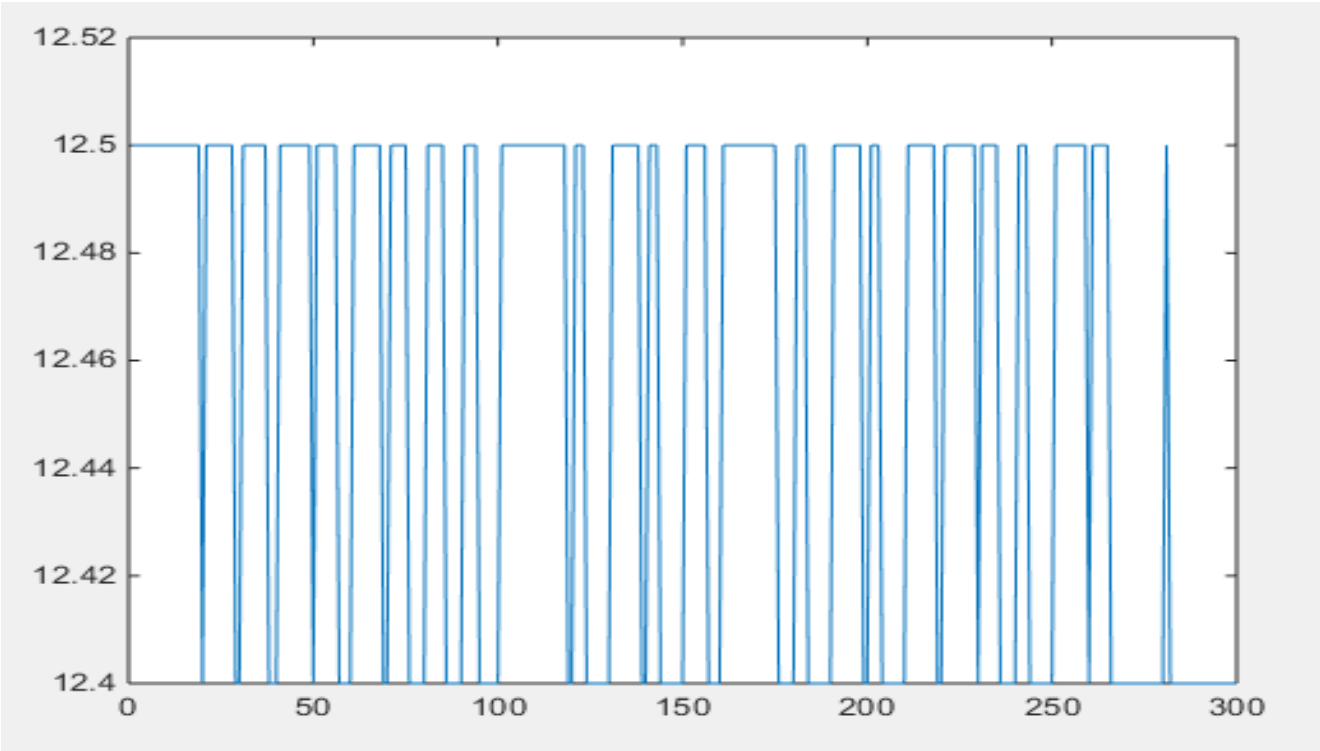


Figure 4.6: Cross-section area variation for the secondary for each step (in mm²)

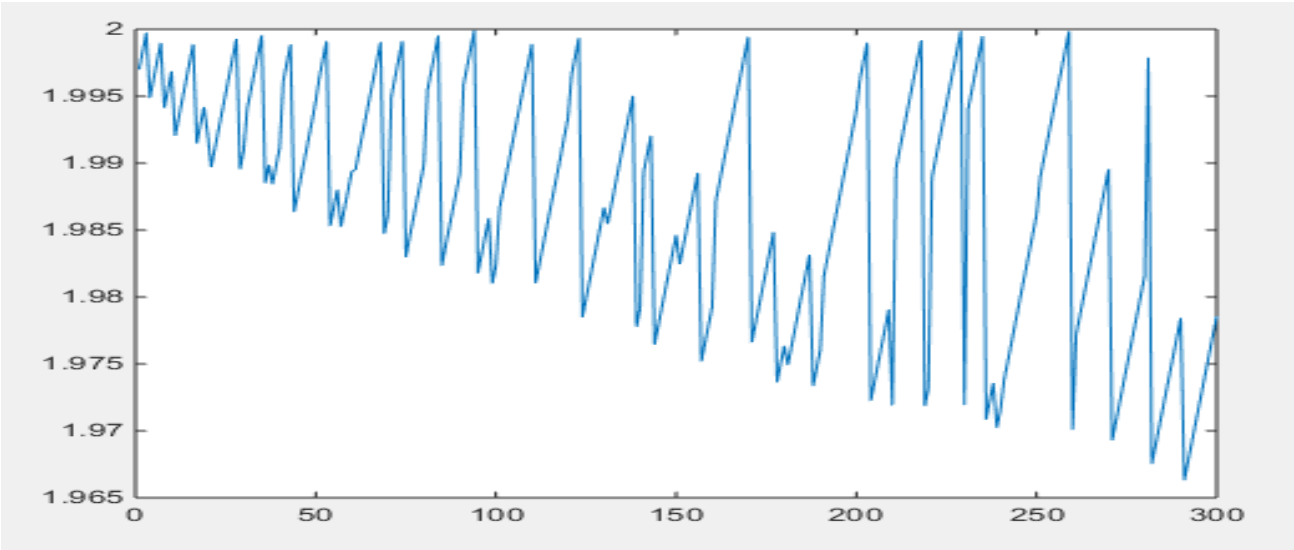


Figure 4.7: Output power variation for each step (in kW)

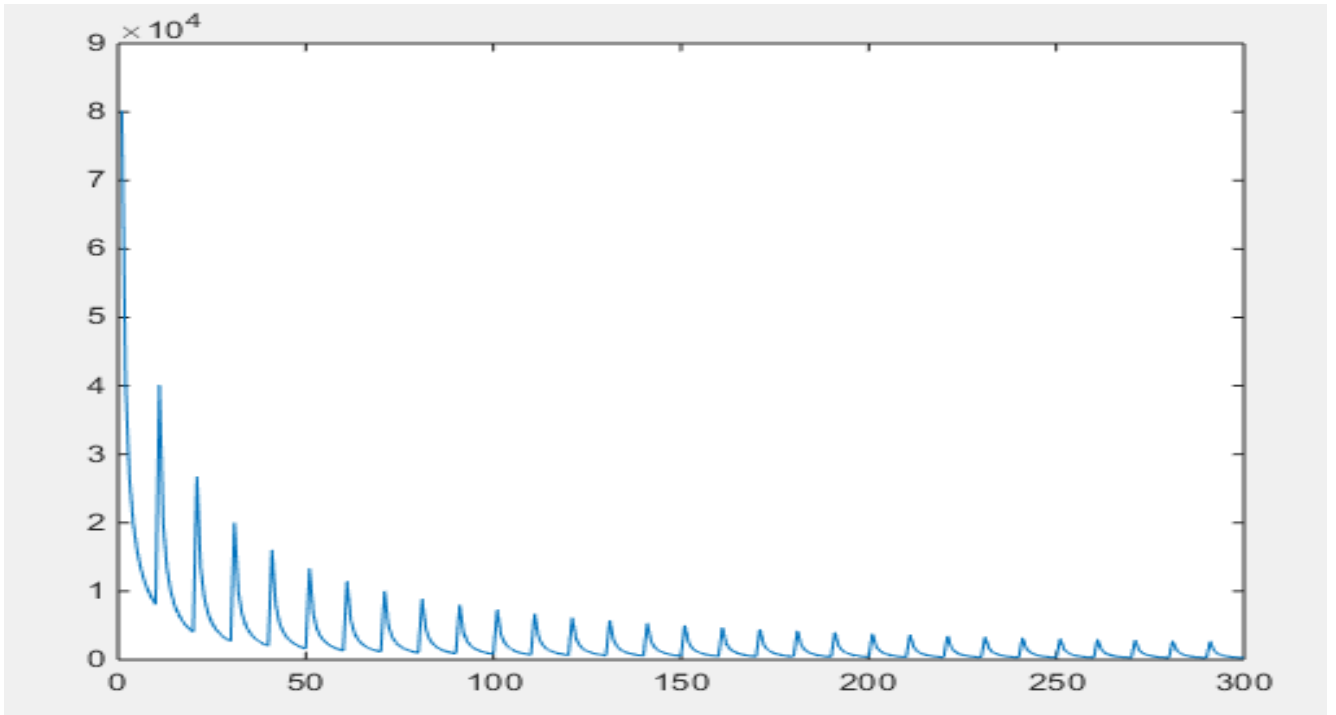


Figure 4.8: Variation of resonance frequency in kHz

Results show that the technique produces possible solution for each set of turn numbers. A true solution should be selected among these results to build the real system. However, although a low switching frequency is targeted, it seems that it is not attained due to some fault in the equations. Therefore, the data given in (Sallan et al., 2009) will be used in the remaining of the chapter.

4.3. Design of a 2 kW System

In (Sallan et al., 2009) a design for a 2 kW system is given. The topology is selected as rectangular coil structure with a maximum frequency of 20 kHz. When the methodology presented in this chapter is applied, the optimum solution was obtained with S-S compensation. The results are shown in Table 4.4. The coil dimensions were found to be $a_1 = 0.4 \text{ m}$, $b_1 = 0.8 \text{ m}$, $a_2 = 0.4 \text{ m}$ and $h = 0.15 \text{ m}$.

Table 4.4: Results of coil parameters by using MATLAB Code

Parameters (Units)	Values
N_1	27
N_2	7
$V_L(V)$	50
$S_1(mm^2)$	2.5
$S_2(mm^2)$	10
$R_1(\Omega)$	0.4
$R_2(\Omega)$	0.02
$L_1(H)$	$14.6e^{-0.4}$
$L_2(H)$	$6.1e^{-0.5}$
P_L	2000
$f_0(KHz)$	19.8
$\eta(\%)$	95
$V_{C1}(V)$	2019
$V_{C2}(V)$	305
$I_p(A)$	10.5
$I_s(A)$	40
$C_2(\mu F)$	$4.3e^{-0.008}$
$C_1(\mu F)$	$1.054e^{-0.006}$
Q_p	10.7
Q_s	6.1

CHAPTER 5

SIMULATION OF THE SYSTEM

5.1. Introduction

Several power converter topologies are proposed in the literature for the IPT systems but essentially their functions are the same and novelty is on the IPT design rather than the converters. Therefore, simulation work for the IPT system was carried out only for the classical single-phase full bridge topology (Erdem et al., 2015). In this chapter operation of single phase full bridge dc-dc converter is described and the simulation results obtained by MATLAB SIMULINK were presented.

5.2. Single Phase Full Wave Bridge Inverter

The full wave bridge inverter includes two arms, two switches, and anti-parallel (freewheeling) diodes. These are used to provide paths for the reverse currents. The converter topology is given in Figure 5.1. The switches are represented here by name of T_1 , T_2 , T_3 , and T_4 respectively. For each branch the upper and lower switches are turned on and off alternating, with a brief dead time in between the transitions. There is 180° phase shift between the two legs which means diagonal switches conduct together to apply square wave voltage across the load (Siqi et al., 2015).

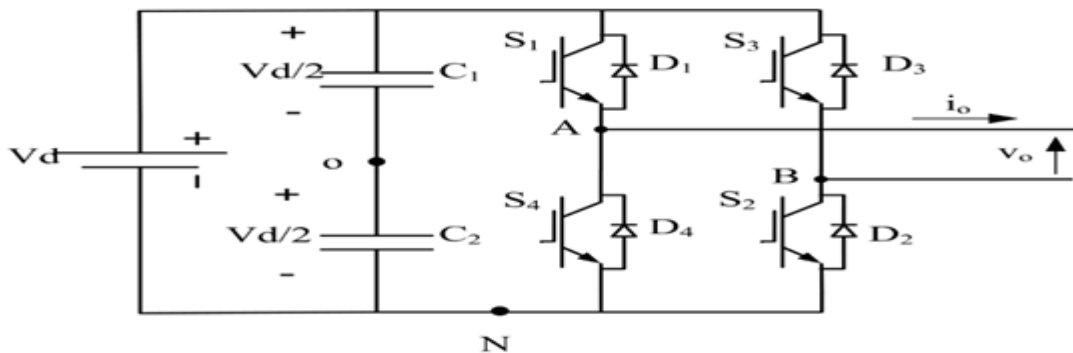


Figure 5.1: Full bridge inverter

The switching combinations and resulting load voltages are listed in Table 5.1.

Table 5.1: Combinations of switches and output voltage

T₁	T₂	T₃	T₄	VA	VB	VAB
On	Off	Off	On	$V_S/2$	$-V_S/2$	$+V_S$
Off	On	On	Off	$V_S/2$	$V_S/2$	$-V_S$
On	Off	On	Off	$V_S/2$	$-V_S/2$	0
Off	On	Off	On	$-V_S/2$	$V_S/2$	0

5.3. Simulated Circuit

The circuit that was used in the simulations is shown in Figure 5.2. The circuit parameters are as follows:

$$L_1 = 1.46mH$$

$$L_2 = 61\mu H$$

$$C_1 = 43.7nF$$

$$C_2 = 1.05nF$$

These parameters are part of those given at the end of Chapter 4. The switching frequency is 20 kHz which the resonance frequency of the LC circuits.

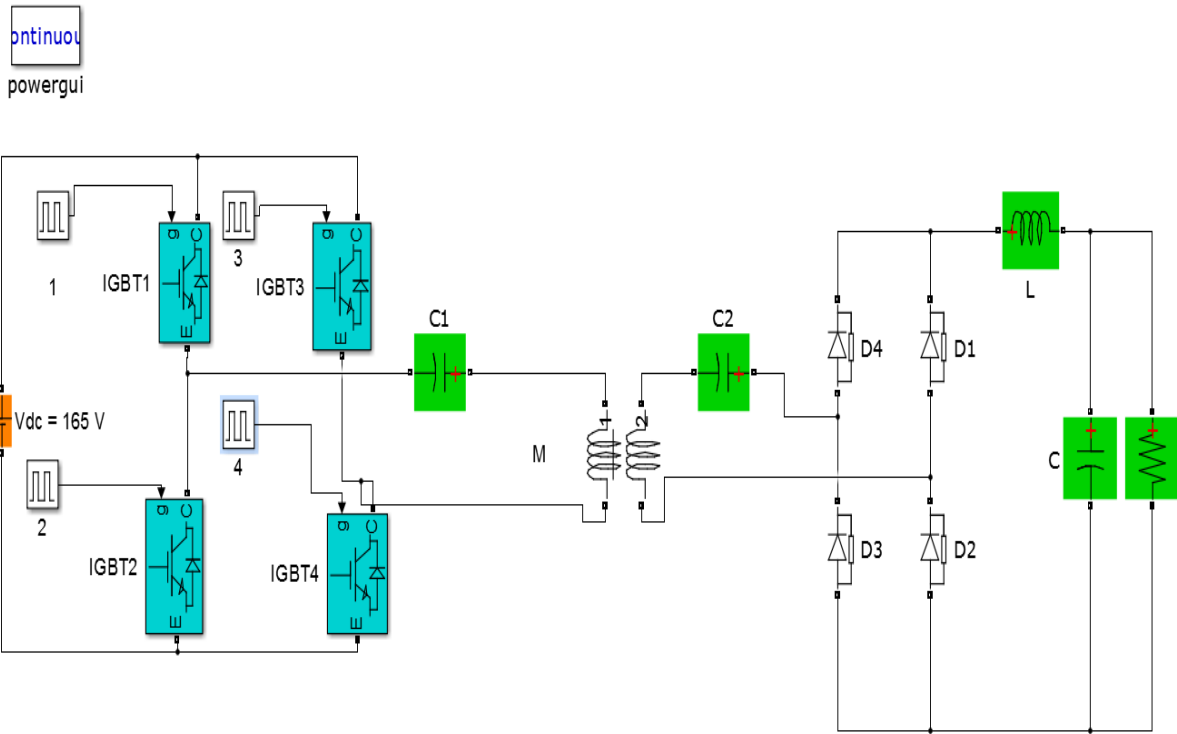


Figure 5.2: Simulated circuit

The primary capacitor is in resonance with the inductance of the transformer. The transformer is defined as a coupled inductor with the inductance parameters given above. The coupling factor is taken as 0.5.

5.4. Simulation Results

Results obtained from the simulation are given in Figures 5.3-5.6. The square wave voltage generated by the inverter is shown in Figure 5.3. The frequency of this voltage is 20 kHz, which is the resonance frequency of the primary. In Figure 5.4, the currents in the primary and secondary are shown. As seen in the figure the currents are nearly sinusoidal at the resonance frequency of 20 kHz. In Figure 5.5 primary capacitor voltage is shown. In Figure 5.5 the secondary side capacitor is given. As expected the voltages can increase significantly meaning special capacitors are required for this application. Finally output voltage is shown in Figure 5.6. The load of this circuit can be replaced with a battery charging system to simulate the real one.

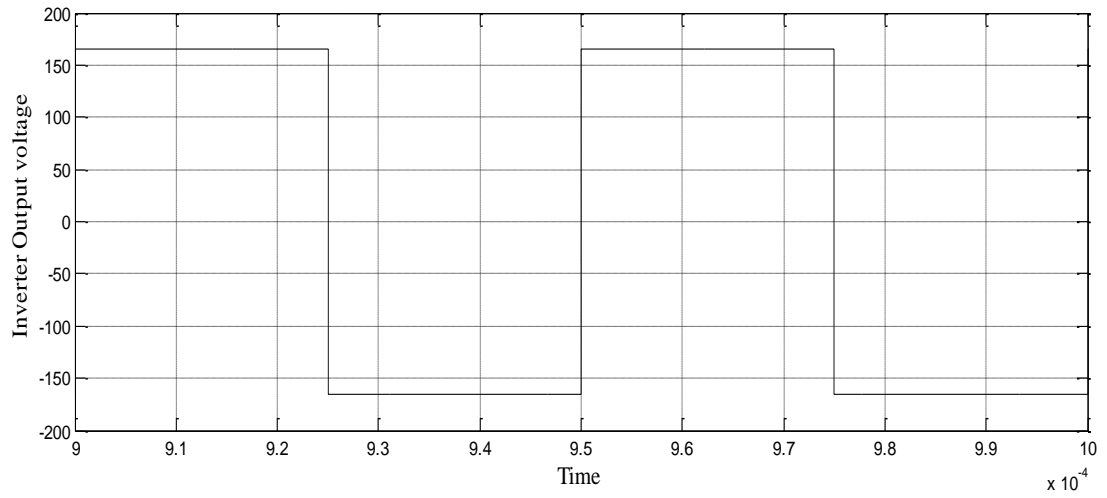


Figure 5.3: Inverter output voltage

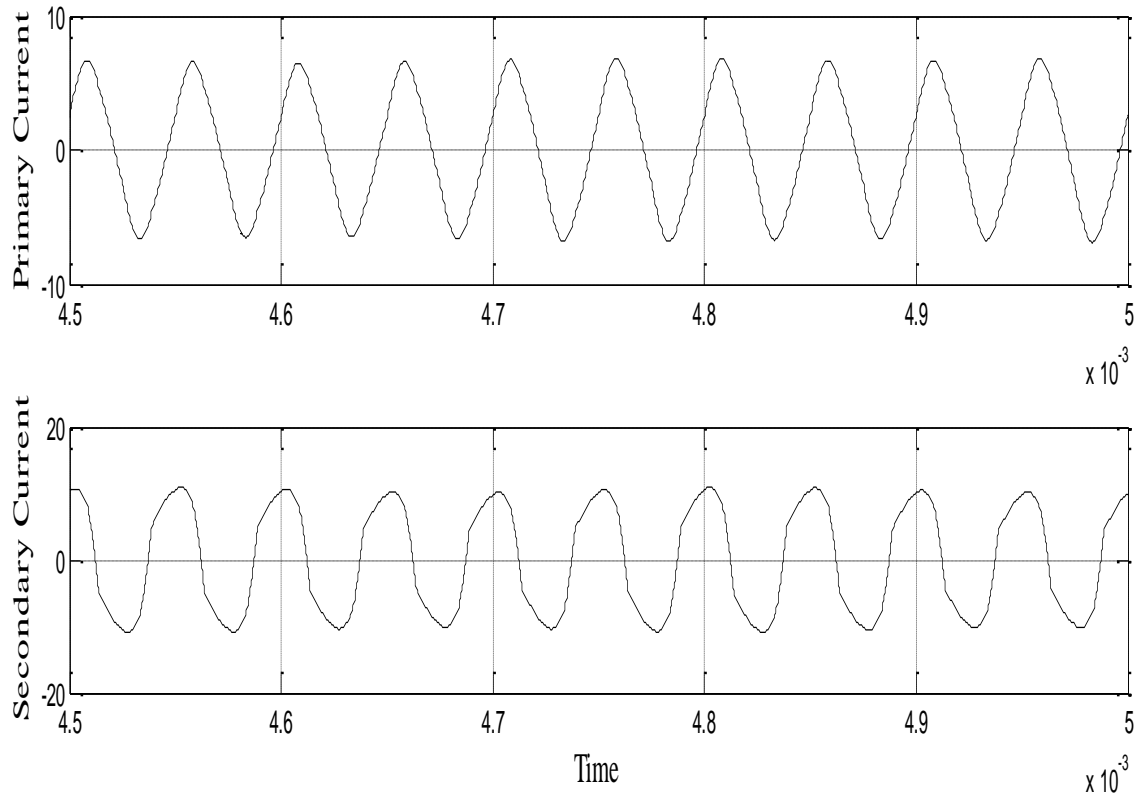
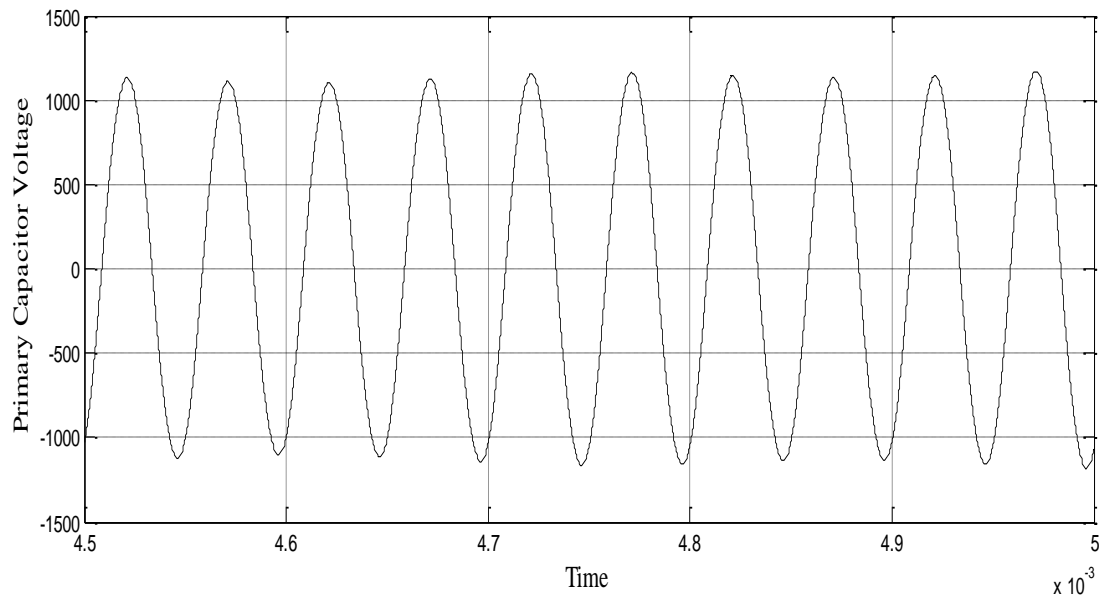
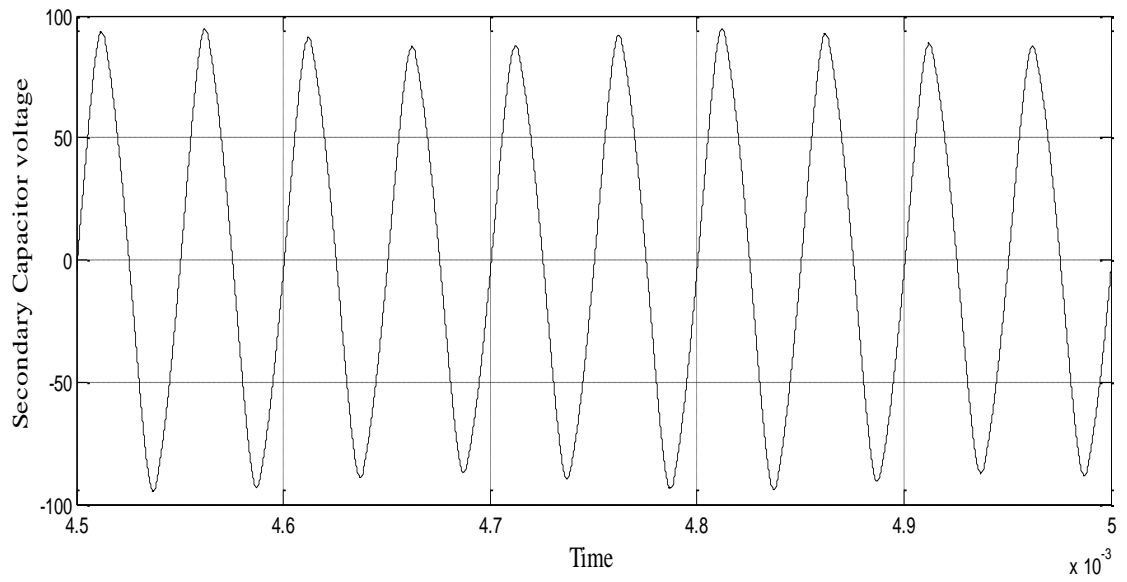


Figure 5.4: Primary and secondary currents



(a) Primary voltage



(b) Secondary voltage

Figure 5.5: Capacitor voltages

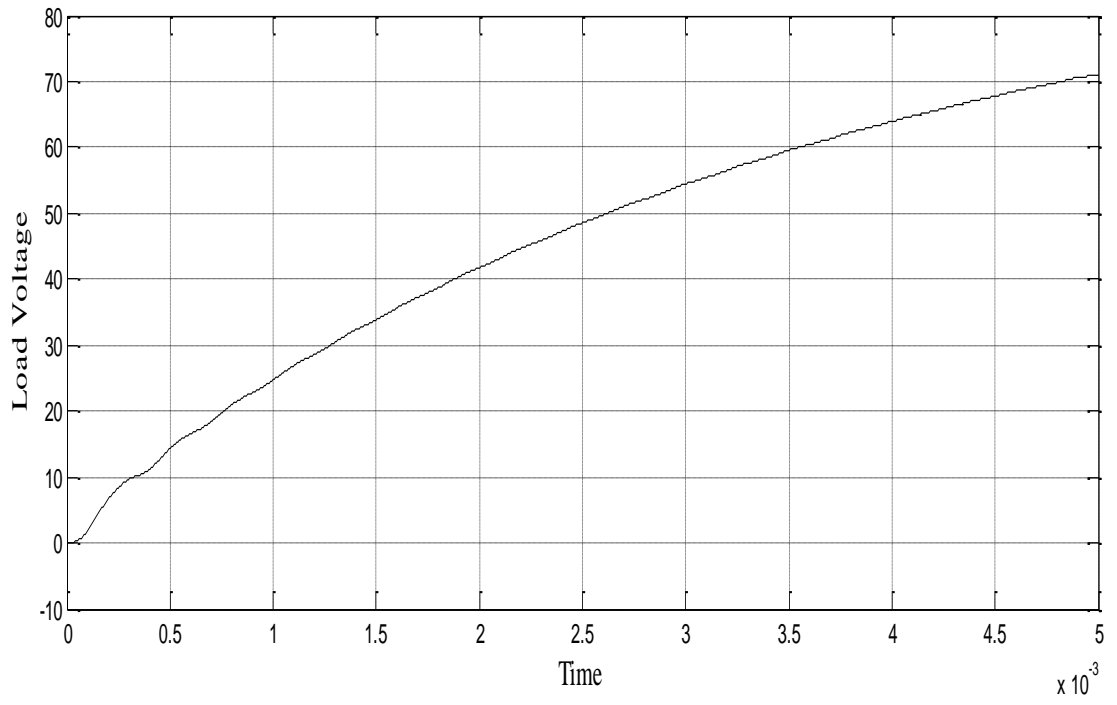


Figure 5.6: Load Voltage

CHAPTER 6

CONCLUSION AND SUGGESTION FOR FUTURE WORK

Inductive power transfer is a promising technology with several possible applications. In this thesis its use for battery charging is investigated. Principles of inductive power transfer were presented and components of IPT systems are described. Coil design and different coil structures were discussed. Finally, a single phase 2 kW system was simulated and results were presented.

In IPT systems power is transferred between the coils of the system. The coils are not around the same core and there is a distance between the coils making the system a loose coupled one. In order to transfer the power efficiently resonance concept should be utilized. There are four classical topologies and also new proposed ones such as LCL topology. The one presented here uses series-series compensation topology, which is adequate for battery charging applications. However, the results show that capacitor voltages increase tremendously and this requires special capacitors. Therefore, LCL topology needs to be utilized instead of the classical series one.

The work presented in this thesis is just an introduction to the concept. In the future LCL type compensation should be studied. Also, comparison of different compensation topologies should be done for the same power level.

Another subject that should be studied is the control of the system. The system was run on open-loop control but it needs to be improved. There are different control topologies presented in the literature and double-side control seems to be very promising. Also hybrid control algorithms, taking care of the duty cycle control and zero phase angle control at the same time can be very interesting. There are already papers investigating this issue.

One final possibility for the future is investigating the operation of different converter topologies, especially multilevel converter topologies as they could provide a good power factor and high powers necessary for some applications

REFERENCES

- Aditya, K., & Willismond, S. S. (2014). Design considerations for loosely coupled inductive power transfer (IPT) system for electric vehicle battery charging-A comprehensive review. *In Proceedings of IEEE International Conference on Transportation Electrification and Expo* (pp.1-6). Dearborn: IEEE.
- Asa, K., E., Colak, K., Bojarski, M., & Czarkowski, D. (2015). A novel multi-level phase controlled resonant inverter with common mode capacitor for wireless EV chargers. *In Proceedings of IEEE International Conference on Transportation Electrification and Expo* (pp.1-6). Dearborn: IEEE.
- Bhudia, M., Boys, J. T., Covic, G.A., & Huang, C. Y. (2013). Development of a single- sided flux magnetic coupler for electric vehicle IPT charging systems. *IEEE Transactions on Industrial Electronics*, 60(1)318-328.
- Bhudia, M., Covic, G., & Boys, J. (2010). A new IPT magnetic coupler for electric vehicle charging systems. *In Proceedings of IECON 2010- 36th Annual Conference on IEEE Industrial Electronics Society* (pp.2487-2492). Glendale: IEEE.
- Chao, Y.H., Sheih, J. J., Pan, C. T., & Shen, W. C. (2007). A closed-form oriented compensator analysis for series-parallel loosely coupled inductive power transfer systems. *In Proceedings of IEEE International Conference on Power Electronics Specialists Conference* (pp.1215-1220). Orlando: IEEE
- Esser, A., & Skudelny, H.C. (1991). A new approach to power supplies for robust. *IEEE Transactions on Industrial Electronics*, 27(5), 872-875.
- Hingorani, N. G., & Gyugyi, L. (2000). Understanding FACTS: concepts and technology of flexible AC transmission systems. United States: Wiley-IEEE press.
- Kalwar, K. A., Amir, M., & Mekhilaf, S. (2015). Inductively coupled power transfer (ICPT) for electric vehicle charging-A review. *Renewable and Sustainable Energy Reviews* ,47, 462-475.

- Lee, B. S., & Han, K.H. (2005). Modeling and analysis of IPT system used for PRT. *In Proceedings of IEEE International Conference on Electric Machines and Systems* (pp. 839-842). Perth: IEEE.
- Li, S., & Mi, C. C. (2015). Wireless power transfer for electric vehicle applications. *IEEE journal of emerging and selected topics in power electronics*, 3(1), 4-17.
- Ruehli, A.E., Antonini, G., & Jiang, L. (2012). Skin-effect model for round wires in PEEC. *In Proceedings of IEEE International Conference on Electromagnetic Compatibility* (pp.1-6). Rome: IEEE.
- Sallán, J., Villa, J.L., Llombart, A., & Sanz, J.F.(2009). Optimal design of ICPT systems applied to electric vehicle battery charge. *IEEE Transactions on Industrial Electronics*, 56(6), 2140-2149.
- Sergeant, P., & Van den Bossche, A. (2008). Inductive coupler for contactless power transmission. *IET Electric Power Applications*, 2(1), 1-7
- Wang, C. S., Covic, G. A., & Stielau, O. H. (2004). Power transfer capability and Bifurcation Phenomena of loosely coupled inductive power transfer systems. *IEEE Transactions on Industrial Electronics*, 51(1), 148-157.
- Wang, C. S., Stielau, O. H., & Covic, G.A. (2000). Load models and their application in the design of loosely coupled inductive power transfer systems. *In Proceedings of IEEE International Conference on Power System Technology* (pp. 1053-1058). Perth: IEEE.
- Wang, C. S., Stielau, O. H., & Covic, G.A. (2005). Design consideration for a contactless electric vehicle battery charger. *IEEE Transactions on Industrial Electronics*, 52(5), 1308-1314.
- Wu, H. H., Golchrist, A., Sealy, K. D., & Bronson, D. (2012). A high efficiency 5kW inductive charger for EV using dual side control. *IEEE Transactions on Industrial Informatics*, +(3), 585-595.

APPENDICES

APPENDIX 1 SOURCE CODE

A.1 Calculations for Self & Mutual Inductance for Rectangular Geometry

Although spiral circular geometry has a better coupling, rectangular geometry is more tolerant to misalignment and is preferred for static IPT systems. In this chapter, design equations for rectangular coils are given.

Rectangular coil structure and dimensions are given in Figure A.1.

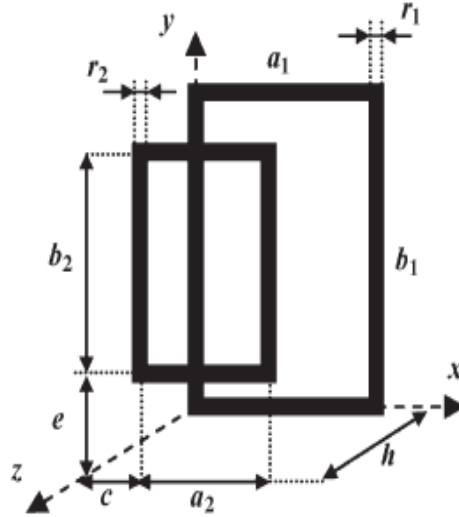


Figure A.1: Rectangular coils parameters dimension and position (Sallan et al., 2009)

Inductance calculations for rectangular geometry are not straight forward but approximate formulas can be obtained by using Neumann's Expressions (Sallan et al., 2009). These formulas are given below for a coil of N_1, N_2 turns in the primary and secondary.

$$L = \frac{\mu_0}{4\pi} N^2 \oint_{\gamma_1} \oint_{\gamma_2} \frac{dl dl'}{r} \quad (4.1)$$

$$L_i = \mu_0 / \pi N_i^2 [a_i \cdot \ln 2a_i b_i / r_i (a_i + \sqrt{a_i^2 + b_i^2}) + b_i \cdot \ln 2a_i b_i / r_i (b_i + \sqrt{a_i^2 + b_i^2}) - 2(a_i + b_i - \sqrt{a_i^2 + b_i^2}) + 0.25(a_i + b_i)] \quad (4.2)$$

where, r_i is the equivalent radius of winding and defined as

$$r_i = \sqrt{N_i S_i / \pi} \quad (4.3)$$

Winding resistance is given as

$$R_i = \rho_{Cu} N_i \times 2(a_i + b_i) / S_i \quad (4.4)$$

$i_1 = 1$ is used for primary winding and $i_2 = 2$ is used for the secondary winding. Both of the coils are wound by using Litz wire to eliminate the skin effects.

Mutual inductance can be calculated in a similar way. Equation (4.5) gives the formula to calculate the mutual inductance.

$$M = \frac{\mu_0}{4\pi} N_1 N_2 \oint_{\gamma_1} \oint_{\gamma_2} \frac{dl dl'}{r} \quad (4.5)$$

Equation (4.6) gives the results of this equation for the case where there may be misalignments between the coils (SALLÁN et al., 2009).

More precise values can be done by using finite element program (FEP).

$$\begin{aligned}
M = & \frac{\mu_0}{4\pi} N_1 N_2 \times \left[\left[d \ln \left(\frac{d \sqrt{h^2 |(t)^2| d^2}}{d + \sqrt{h^2 + d^2 + q^2}} \right) \right] \right] + h \ln \frac{g + \sqrt{h^2 + q^2 + g^2}}{g + \sqrt{h^2 + q^2 + (-t)^2}} + c \ln \\
& \frac{(-c) + \sqrt{h^2 + q^2 + c^2}}{(-c) + \sqrt{h^2 + c^2 + (-t)^2}} + m \ln \frac{(-m) + \sqrt{h^2 + (-t)^2 + m^2}}{(-m) + \sqrt{h^2 + m^2 + q^2}} \\
& + \sqrt{h^2 + m^2 + d^2} - \sqrt{h^2 + q^2 + g^2} - \sqrt{h^2 + q^2 + m^2} + \sqrt{h^2 + q^2 + c^2} \\
& + \sqrt{h^2 + (-t)^2 + g^2} - \sqrt{h^2 + (-t)^2 + d^2} + \sqrt{h^2 + (-t)^2 + m^2} - \sqrt{h^2 + (-t)^2 + c^2} \\
& - \left[d \ln \left(\frac{d + \sqrt{h^2 + (-p)^2 + d^2}}{d + \sqrt{h^2 + d^2 + e^2}} \right) \right] + \left[g \ln \left(\frac{(h) + \sqrt{h^2 + e^2 + g^2}}{d + \sqrt{h^2 + |h^2| + (p)^2}} \right) \right] + \\
& c \ln \left(\frac{(-c) + \sqrt{h^2 + e^2 + c^2}}{(-c) + \sqrt{h^2 - c^2 + (-p)^2}} \right) + m \ln \left(\frac{(-m) + \sqrt{h^2 + (-p)^2 + m^2}}{(-m) + \sqrt{h^2 + m^2 + e^2}} \right) \\
& + \sqrt{h^2 + e^2 + d^2} - \sqrt{h^2 + e^2 + g^2} - \sqrt{h^2 + e^2 + m^2} - \sqrt{h^2 + e^2 + c^2} \\
& + \sqrt{h^2 + (-p)^2 + g^2} - \sqrt{h^2 + (-p)^2 + d^2} + \left| \sqrt{h^2 |(p)^2| m^2} \sqrt{h^2 |(p)^2| c^2} \right| + t \ln \left(\frac{t \sqrt{h^2 |(g)^2| t^2}}{t + \sqrt{h^2 + t^2 + c^2}} \right) \\
& + p \ln \left(\frac{p + \sqrt{h^2 + p^2 + c^2}}{p + \sqrt{\sqrt{h^2 + (-g)^2 + p^2}}} \right) \\
& + e \ln \left(\frac{(-e) + \sqrt{h^2 + e^2 + c^2}}{(-e) + \sqrt{\sqrt{h^2 + e^2 + (-g)^2}}} \right) + q \ln \left(\frac{(-q) + \sqrt{h^2 + (-g)^2 + q^2}}{(-q) + \sqrt{\sqrt{h^2 + c^2 + q^2}}} \right) \\
& + \sqrt{h^2 + c^2 + t^2} - \sqrt{h^2 + c^2 + p^2} - \sqrt{h^2 + c^2 + q^2} - \sqrt{h^2 + e^2 + c^2} \\
& + \sqrt{h^2 + (-g)^2 + p^2} - \sqrt{h^2 + (-g)^2 + t^2} + \sqrt{h^2 + (-g)^2 + q^2} - \sqrt{h^2 + (-g)^2 + e^2} \\
& - \left[t \ln \left(\frac{t + \sqrt{h^2 + (-d)^2 + t^2}}{t + \sqrt{\sqrt{h^2 + t^2 + m^2}}} \right) \right] + p \ln \left(\frac{p + \sqrt{h^2 + m^2 + p^2}}{p + \sqrt{\sqrt{h^2 + (-d)^2 + p^2}}} \right) + e \ln \left(\frac{(-e) + \sqrt{h^2 + e^2 + m^2}}{(-e) + \sqrt{\sqrt{h^2 + e^2 + (-d)^2}}} \right)
\end{aligned}$$

$$\begin{aligned}
& +q \ln \left(\frac{(-q) + \sqrt{h^2 + (-d)^2 + q^2}}{(-q) + \sqrt{h^2 + m^2 + q^2}} \right) + \sqrt{h^2 + m^2 + t^2} - \sqrt{h^2 + m^2 + p^2} \\
& - \sqrt{h^2 + m^2 + q^2} + \sqrt{h^2 + e^2 + m^2} + \sqrt{h^2 + (-d)^2 + p^2} - \sqrt{h^2 + (-d)^2 + t^2} \\
& + \sqrt{h^2 + (-d)^2 + q^2} - \sqrt{h^2 + (-d)^2 + e^2}
\end{aligned} \tag{4.6}$$

APPENDIX 2 SOURCE CODE

Source codes for the coil design used in this thesis are given

2.1. Main Program

```
%%%%%%%%%%
%%%%%%%%%%
```

```
clearall
clc
kk=0;
%DIMENSIONS
a=[0.1 0.1];
b=[0.2 0.1];
z=0.15;

PLoad=2000; %Desired load power

N1max=30;
dKw=0.1;
N2max=10;
deltamax=4e6;

N=[1 1];
Kw0=1;
S10=1e-06;
S20=1e-06;
S=[S10 S20];
delS=1e-07;
Kw=Kw0;
% INDUCTANCE COMPUTATIONS
[L,M]=LMcalculation(N,S,a,b);
% END OF INDUCTANCE COMPUTATIONS

%IMPEDANCE, CURRENT, VOLTAGE AND POWER CALCULATIONS
while (2) %TURN NUMBER LOOP
while (1) %CROSS-SECTION AREA LOOP
%%% Table 1 equations
[Pcomp,PL,Qp,Qs,delta1,delta2,w0]=table1eq(Kw,N,M,L,a,b,S,PLoad);
f=w0/(2*pi());
ifPcomp>(1.0*PLoad)
Kw=Kw+dKw;
elseif(delta1>deltamax)
S(1)=S(1)+delS;
Kw=Kw0;
[L,M]=LMcalculation(N,S,a,b);
elseif(delta2>deltamax)
S(2)=S(2)+delS;
```

```

                                Kw=Kw0;
                                [L,M]=LMcalculation(N,S,a,b);

else
kk=kk+1;
solution(kk,1)=N(1);
solution(kk,2)=N(2);
solution(kk,3)=S(1)*1e06;      %mm2
solution(kk,4)=S(2)*1e06;      %mm2
solution(kk,5)=Pcomp/1000;      %W
solution(kk,6)=f/1000;         %kHz
break
end

end%end of loop 1 (cross-section adjustment)

if N(2)<N2max
N(2)=N(2)+1;
                                S=[S10 S20];
                                Kw=Kw0;
                                [L,M]=LMcalculation(N,S,a,b);

else
N(1)=N(1)+1;
if N(1)>N1max
N(1)=N(1)-1;
Nprint=N
                                Sprint=S

fprint=f
PLprint=PL
break
else
N(2)=1;
                                S=[S10 S20];
                                Kw=Kw0;
                                [L,M]=LMcalculation(N,S,a,b);

end
end
end
%end of loop 2 (turn number adjustment)

```

APPENDIX 3 SOURCE CODE

3.1. Code of Table 1 Equations

```
%%%%%%%%%%
%%%%%%%%%%
```

```
function [Pcomp, PL, Qp, Qs, delta1, delta2, w0]=table1eq(Kw, N, M, L, a, b, S, PLoad)
```

```
% Table 1 equations
```

```
VLoad=50;
V1=165;
Rload=PLoad/VLoad^2;
Rocu=1.72*10^(-8);
V1=165;

R=zeros(1,2);
C=zeros(1,2);

for i=1:2
R(i)=Rocu*N(i)*(2*(a(i)+b(i))/S(i));
end
wmin=sqrt(R(1)*(R(2)+Rload))/M;
w0=Kw*wmin;
f=w0/(2*pi());
C(1)=1/(w0^2*L(1));
C(2)=1/(w0^2*L(2));
Zss=complex(R(1),(L(1)*w0-
(1/(C(1)*w0))))+(w0^2*M^2)/complex(R(2)+Rload,(L(2)*w0-(1/(C(2)*w0))));
I1=V1/Zss;
Ip=I1;
absIp=abs(Ip);
Ic1=Ip;
Vc1=I1/complex(0,C(1)*w0);
Isn=Ip*complex(0,w0*M);
Isd=complex((R(2)+Rload),(w0*L(2)-1/(w0*C(2))));
Is=Isn/Isd;
I2=Is;
Ic2=Is;
Vc2=Is/complex(0,(C(2)*w0));
Vload=Rload*I2;
aVload=abs(Vload);
% PL is the real load power
PL=aVload^2/Rload;
Qp=(L(1)*Rload)/(w0*M^2);
Qs=(w0*L(2))/Rload;
% Pcomp is the expected power for a compensated system
Pcomp=(w0*M^2*Qs*absIp^2)/L(2);
delta1=abs(I1)/S(1);
delta2=abs(I2)/S(2);
```

APPENDIX 4 SOURCE CODE

4.1. Equations for L and M Calculations

```

function [L,M]=LM calculation(N,S,a,b)

%Calculation of Inductances
r=zeros(1,2);
L=zeros(1,2);
z=0.15;
m0=4*pi*(10^-7);
for i=1:2
r(i)=sqrt((N(i)*S(i))/pi);

L(i)=m0/pi*N(i)^2*(a(i)*log(2*a(i)*b(i)/(r(i)*(a(i)+sqrt(a(i)^2+b(i)^2)))
+b(i)*log(2*a(i)*b(i)/(r(i)*(a(i)+sqrt(a(i)^2+b(i)^2))))-
2*(a(i)+b(i)-sqrt(a(i)^2+b(i)^2))+0.25*(a(i)+b(i)));
    F1=-(m0)/(4*pi)*(b(1)/2+b(2)/2)*log((-
(b(1)/2+b(2)/2)+sqrt((b(1)/2+b(2)/2)^2+(a(1)/2-
a(2)/2)^2+z^2))/(b(1)/2+b(2)/2)+sqrt((b(1)/2+b(2)/2)^2+(a(1)/2-
a(2)/2)^2+z^2)-(b(1)/2-b(2)/2)*log((-b(1)/2-b(2)/2)+sqrt((b(1)/2-
b(2)/2)^2+(a(1)/2-a(2)/2)^2+z^2))/(b(1)/2-b(2)/2)+sqrt((b(1)/2-
b(2)/2)^2+(a(1)/2-a(2)/2)^2+z^2))+2*sqrt((b(1)/2+b(2)/2)^2+(a(1)/2-
a(2)/2)^2+z^2)-2*sqrt((b(1)/2-b(2)/2)^2+(a(1)/2-a(2)/2)^2+z^2));
    F2=(m0)/(4*pi)*(b(1)/2+b(2)/2)*log((-
(b(1)/2+b(2)/2)+sqrt((b(1)/2+b(2)/2)^2+(a(1)/2+a(2)/2)^2+z^2))/(b(1)
/2+b(2)/2)+sqrt((b(1)/2+b(2)/2)^2+(a(1)/2+a(2)/2)^2+z^2)-(b(1)/2-
b(2)/2)*log((-b(1)/2-b(2)/2)+sqrt((b(1)/2-
b(2)/2)^2+(a(1)/2+a(2)/2)^2+z^2))/(b(1)/2-b(2)/2)+sqrt((b(1)/2-
b(2)/2)^2+(a(1)/2+a(2)/2)^2+z^2))+2*sqrt((b(1)/2+b(2)/2)^2+(a(1)/2+a
(2)/2)^2+z^2)-2*sqrt((b(1)/2-b(2)/2)^2+(a(1)/2+a(2)/2)^2+z^2));
    F3=-(m0)/(4*pi)*(a(1)/2+a(2)/2)*log((-
(a(1)/2+a(2)/2)+sqrt((a(1)/2+a(2)/2)^2+(b(1)/2-
b(2)/2)^2+z^2))/(a(1)/2+a(2)/2)+sqrt((a(1)/2+a(2)/2)^2+(b(1)/2-
b(2)/2)^2+z^2)-(a(1)/2-a(2)/2)*log((-a(1)/2-a(2)/2)+sqrt((a(1)/2-
a(2)/2)^2+(b(1)/2-b(2)/2)^2+z^2))/(a(1)/2-a(2)/2)+sqrt((a(1)/2-
a(2)/2)^2+(b(1)/2-b(2)/2)^2+z^2))+2*sqrt((a(1)/2+a(2)/2)^2+(b(1)/2-
b(2)/2)^2+z^2)-2*sqrt((a(1)/2-a(2)/2)^2+(b(1)/2-b(2)/2)^2+z^2));
    F4=(m0)/(4*pi)*(a(1)/2+a(2)/2)*log((-
(a(1)/2+a(2)/2)+sqrt((a(1)/2+a(2)/2)^2+(b(1)/2+b(2)/2)^2+z^2))/(a(1)
/2+a(2)/2)+sqrt((a(1)/2+a(2)/2)^2+(b(1)/2+b(2)/2)^2+z^2)-(a(1)/2-
a(2)/2)*log((-a(1)/2-a(2)/2)+sqrt((a(1)/2-
a(2)/2)^2+(b(1)/2+b(2)/2)^2+z^2))/(a(1)/2-a(2)/2)+sqrt((a(1)/2-
a(2)/2)^2+(b(1)/2+b(2)/2)^2+z^2))+2*sqrt((a(1)/2+a(2)/2)^2+(b(1)/2+b
(2)/2)^2+z^2)-2*sqrt((a(1)/2-a(2)/2)^2+(b(1)/2+b(2)/2)^2+z^2));
    M=N(1)*N(2)*2*(F1+F2+F3+F4);
end

```